New Applications of Fluorescence Correlation Spectroscopy for Early Detection of Apoptosis in Cells

By

Divya Iyer, M.Sc.

A Thesis

In

Chemistry

Submitted to the Graduate Faculty

of Texas Tech University in

Partial Fulfillment of

the Requirements for

the Degree of

MASTER OF SCIENCE

Approved

Dr. Dimitri Pappas
Chair of Committee

Dr. Jon Thompson

Dr. Dominick Joseph Casadonte
Interim Dean of the Graduate School

August, 2013

ACKNOWLEDGEMENTS

"Each of us has cause to think with deep gratitude of those who have lighted the flame of knowledge within us"

- Albert Schweitzer

Firstly, I wish to express my heartfelt gratitude to my advisor Dr. Dimitri Pappas who introduced me to this exciting field of research related to 'Microfluidics and Fluorescence Microscopy'. I am ever indebted to him for his constant encouragement, enthusiasm, guidance and support in every form throughout my research at Texas Tech University. I also want to thank him for giving me the rare opportunity to become the head teaching assistant (TA) for analytical chemistry labs and gain hands-on experience with troubleshooting various analytical instrumentation and authoring SOPs for experiments.

I would like to thank the past and present members of the Pappas Group; Peng Li, Yu Tian, Yan Liu, Michelle Martinez, Grishma Khanal, Yan Gao, Meicong Dong and Himali Somaweera for being amazing colleagues, mentors and friends who always created a positive and pleasant work environment around me. I would specifically like to thank Michelle for guiding and mentoring me with Fluorescence Correlation Spectroscopy (FCS) techniques, Yan Liu and Yan Gao for giving me training on chip fabrication and cell culturing. I would also like to thank Peng Li to train me on Flow Cytometry and Grishma for the very helpful and frequent brainstorming sessions on biochemical mechanisms.

I would also like to thank my committee member Dr. Jon Thompson for his guidance during my seminar and for teaching me Good Laboratory Practices (GLPs) when I was working as his head TA. I would like to thank Dr. Carol Korzeniewski for giving me the opportunity to pursue my higher studies at the department of chemistry and biochemistry as a transfer student. Had it not been for her confidence in me, I would not have pursued my graduate studies in the US.

Lastly, I would like to thank my family back in India who gave me this rare opportunity and freedom to explore my options abroad and to advance my career in the field of chemistry.

"As we express our gratitude, we must never forget that the highest appreciation is not to utter words, but to live by them"

- J. F. Kennedy

TABLE OF CONTENTS

ABSTRACT

In the present study, early stage apoptosis is explored with high temporal resolution. In addition to monitoring early apoptosis induction in single cells by ultrasensitive confocal fluorescence microscopy (UCFM), the mitochondrial proteins release kinetics was explored. The current study shows development and optimization of a novel, rapid apoptosis assay to explore the earliest changes in cells by the intrinsic apoptosis pathway. We show that early apoptotic changes in the mitochondria begin nearly simultaneously with the addition of an apoptosis-inducing drug, such as staurosporine. With a temporal resolution of five minutes, this non-invasive analytical technique can elucidate the earliest apoptotic events in living cells. Moreover, our results show that the mitochondrial inter-membrane proteins are not involved in the extrinsic pathway of Ramos cells mediated by an anti-CD95 antibody. Additional techniques such as light microscopy, flow cytometry and microfluidic technology were employed to explore ultrasensitive and high throughput detection of apoptosis in cells using confocal fluorescence microscopy. The results of this study help to understand the earliest mechanisms of apoptosis induction in cells and to develop high throughput cell screening using microfluidic technology, enabling new methods of rapid drug testing and dose-response analyses.

LIST OF FIGURES

CHAPTER 1

INTRODUCTION

1.1 Introduction to Apoptosis

Programmed cell death, commonly known as apoptosis, plays a major role in several biological processes such as embryogenesis, aging and in diseases like cancer and muscular dystrophy. [1,2] Apoptosis plays an important role in designing drugs for treatment, diagnosis of diseases such as cancer, elucidating complex molecular mechanisms and so on. There are numerous molecular mechanisms that involve apoptosis in death signals, genetic regulation and activation of effectors.[3] Many existing treatments such as non-steroidal anti-inflammatories and anticancer treatments act through the process of apoptosis.[4]

1.2 Apoptosis Pathways

Apoptosis research started decades ago and since then it has been evolving at a rapid rate with the development of several analytical methods and biological assays. Although most of the proteins involved in various apoptosis mechanisms have been identified, the actual molecular mechanism of these proteins remains unknown.[5] The two main apoptotic pathways are the extrinsic pathway and the intrinsic (mitochondrial) pathway (Figure 1.1). The extrinsic (death receptor) pathway involves the formation of a death-inducing signaling complex (DISC) that initiates the release of active caspases 8 and 10 into the cytosol, beginning the process of apoptosis.[6] Activation of intrinsic pathway occurs through the activation of Bax and Bak

proteins after conversion of Bid to tBid by caspase 8 and 10.[7] This process causes a decrease in mitochondrial membrane potential and the release of several mitochondrial proteins such as Smac/DIABLO and cytochrome c. When cytochrome c combines with Apaf-1 and pro-caspase 9, it forms the apoptosome. Pro-caspase 9 is then converted into caspase 9 that in turn activates caspase 3,7 to further execute the process of apoptosis.[6] Later apoptosis stages include the exposure of phosphatidylserine to the outer membrane and cell shrinkage.[8] Although both the extrinsic and intrinsic pathways are mediated by different mechanisms, ultimately they share a common final phase of activation of caspases 3, 6 and 7.

Due to the complexity of the apoptosis process, there is a need to study protein activity and mechanisms at multiple time points. A detailed discussion of all the methodologies and assays for apoptosis detection used so far is beyond the scope of this research work, but these methods have been reviewed recently.[10] Elmore[9] has given a detailed description of classification of apoptosis assays on the basis of cytomorphological alterations, DNA fragmentation, detection of various caspases, membrane alterations and mitochondrial assays. Figure 1.2 illustrates some of the bioanalytical assays that have been employed to study apoptosis in cells at various stages. Whether the cells are in the early stages of apoptosis (with exposed inner leaflets), intermediate stages (with active caspase activity), or late stages (with extensive DNA fragmentation), there is a need of cell-based assay to detect specific cell death processes across the apoptotic timeline. Most analytical methods are either incapable of high temporal resolution

measurements or are too invasive for dose response and kinetic studies.[10] In order to elucidate earliest apoptosis mechanisms non-invasively, it is important to develop apoptosis assays with high temporal resolution for rapid detection.

1.3 Conclusion

Fluorescence Correlation Spectroscopy (FCS) allows rapid detection of intensity fluctuations in a few minutes time frame after apoptosis is induced in cells. This current work sheds light on some of the earliest assays to detect apoptosis induction in cancer cells in a 30 μL droplet. We demonstrate high throughput screening of flowing cells in a micro-channel using the FCS technique as a means of further improving cell-based apoptosis assays.

The unparalleled sensitivity, high temporal resolution and high throughput demonstrated by our current methods will not only improve apoptosis detection capabilities but can also track patient response to treatments. This work will introduce rapid analyses of single cells for apoptosis to elucidate cancer cell death mechanisms in ways that have not been explored so far. Since no other analytical technique has comparable temporal resolution and sensitivity, the impact of this work is expected to be high.

1.4 References

1. O. Yoshinori, L. Zhonglian, S. Masa-Ai, *The Journal of Histochemistry and Cytometry*, 2003, 38, 275-340.

2. B. Favaloro, N. Allocati, V. Graziano, C. Di Ilio, V. De Laurenzi, *Aging*, 2012, 4, 330-349.

3. A. G. Renehan, C. Booth and C. S. Potten, *BMJ*. 2001, 322, 1536–1538.

4. G. T. Le and G. Abbenante, *Curr Med Chem,* 2005*,* 12, 2963–77.

5. K. Duncan, H. Uwimpuhwe, A. Czibere, D. Sarkar, T. A. Libermann, P. B. Fisher, L. F. Zerbini, *IUBMB Life*. 2012, 7, 636-643.

6. D. Wlodkowic, W. Telford, J. Skommer and Z. Darzynkiewicz, *Methods Cell Biol.* 2011, 103, 55–98.

7. G. Kroemer, L. Galluzzi, and C. Brenner, Physiol Rev. 2007, 87, 99–163.

8. G. M. Salido and J. A. Rosado, Apoptosis: Involvement of oxidative stress and intracellular Ca^{2+} homeostasis, *Springer*, 2009.

9. Susan Elmore, *Toxicologic Pathology*, 2007, 35, 495–516.

10. M. M. Martinez, R. D. Reif and D. Pappas, *Anal Methods*, 2010, 2, 996-1004.

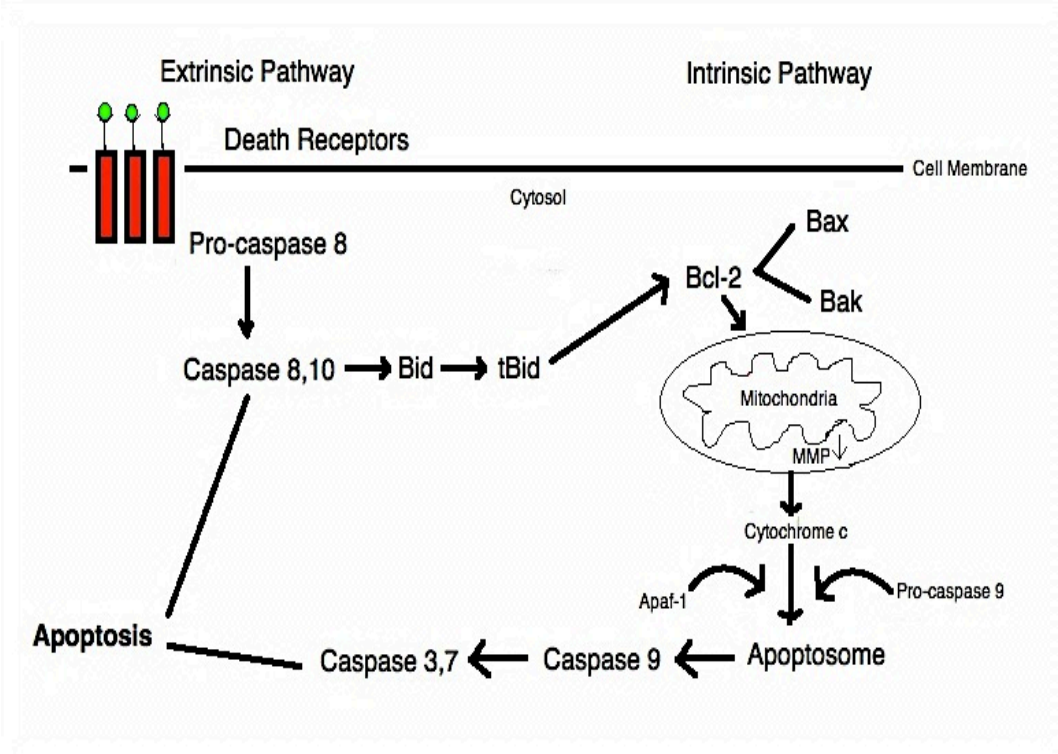

Figure 1.1: Extrinsic and Intrinsic pathways of apoptosis. MMP – Mitochondrial Membrane Potential. Apaf-1 - Apoptotic protease activating factor 1. Bcl-2 – Apoptosis regulator protein. Bax, Bak, Bid, tBid – proapoptotic Bcl-2 family members. The extrinsic pathway begins with the activation of death receptors and pro-caspase 8, which in turn activates caspases 8 and 10 leading to apoptosis and cell death. The intrinsic pathway initiates the formation of mitochondrial outer membrane pore (MOMP) that causes diffusion of mitochondrial proteins into the cellular matrix. This activates cytochrome c and formation of the apoptosome bodies that in turn activates caspases 9, 3 and 7 leading to apoptosis.

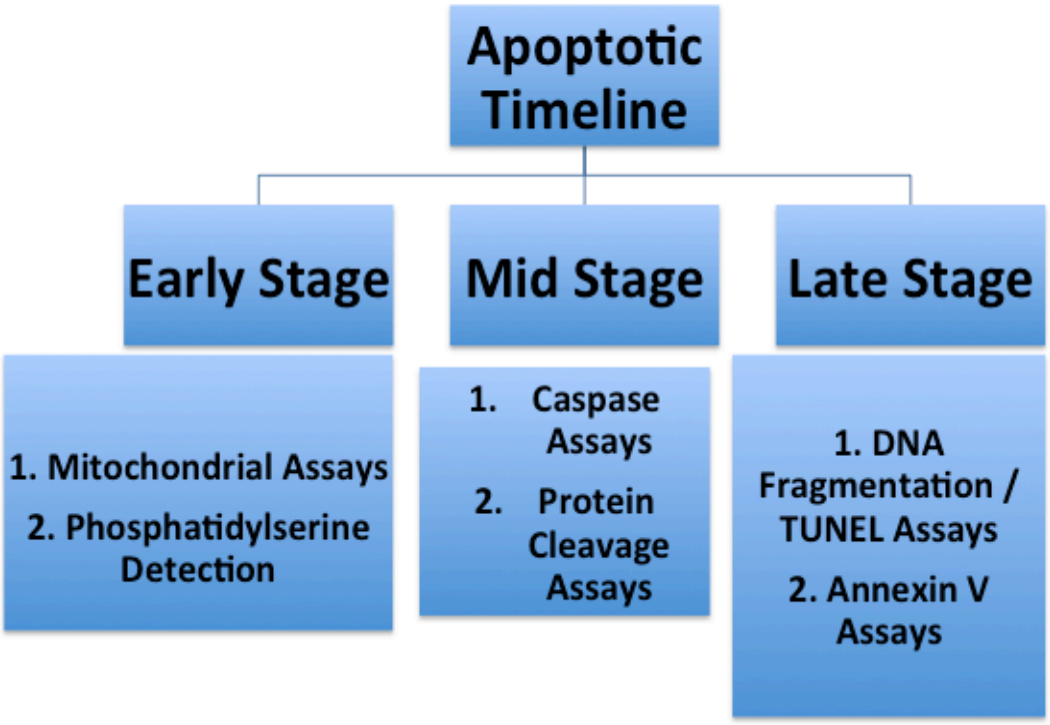

Figure 1.2: Classification of assays used for apoptosis detection across the apoptotic timeline.

CHAPTER 2
INSTRUMENTATION AND THEORETICAL BASIS

2.1 Introduction

Over the past few years, there has been a rapid increase in developing methods that deal with single-molecule interactions within cells. Fluorescence Correlation Spectroscopy (FCS) has given new insights into the kinetics and dynamics of individual molecules in sub-microsecond range. For example, single molecule studies within cells allow us to observe the complex release dynamics of mitochondrial proteins after apoptosis induction. Such observations help elucidate the complex intermolecular biological mechanisms and reactions in an intact cell non-invasively on a nanometer scale.

Various imaging techniques such as Atomic Force Microscopy (AFM), Scanning Tunneling Microscopy (STM) and cryo-Transmission Electron Microscopy (cryo-TEM) have been explored to image subcellular organelles in nanometer range. However, none of these techniques focus on high temporal resolution of the apoptosis assays. FCS has been widely employed to study molecular mobility with very high sensitivity. For the first time the infection pathway of a virus was visualized using single molecule tracking and FCS.[1] Moreover, there are several other biological processes in a live cell that have been monitored and visualized by the aid of FCS.[2-6] It is important to remember that FCS is not used to follow motion of a single molecule, but is used to give an ensemble average of the number of multiple single molecule events from fluorescent molecules present in the probe volume. These single

molecule events can be used to determine the diffusion time of molecules.

In this thesis, FCS has been employed to indirectly investigate the complex release dynamics of mitochondrial proteins after apoptosis induction. For this purpose, a custom built FCS setup was made to allow rapid measurements of fluorescence intensity in live cells with a temporal resolution of 5 minutes. In addition to obtaining the autocorrelation functions, photon counting histograms were employed to monitor intensity fluctuations in various systems as a function of time.

2.2 Fluorescence Correlation Spectroscopy

W. W. Webb and co-workers have explained the theoretical background of FCS in details in early 1970s using a Dynamic Light Scattering analogy.[7-9] FCS obtains correlation from fluorescence intensity fluctuations when a laser beam illuminates a small part of the cell. The major reason for these fluctuations is the transport of the fluorophore through the confocal volume; hence they are widely employed to study the Brownian movement of fluorophores in the probe volume. In this current study, Ramos cells were induced to undergo apoptosis by staurosporine via the intrinsic response mechanism and were stained with MitoTracker Deep Red, a mitochondrial probe. Figure 2.1 shows the concept of these measurements and how an autocorrelation function arises from the mobility of mitochondrial proteins.

The FCS 3D Diffusion Model is given by;[10]

$$G_{3D}(t) = \frac{1}{N}\left(1+\frac{\tau}{\tau_D}\right)^{-1}\left(1+\frac{\tau}{\tau_D * S^2}\right)^{-1/2} \quad (2.1)$$

Where $G_{3D}(\tau)$ is the autocorrelation function for a 3D fit, N is the average number of molecules in the probe volume, S is the structure parameter that characterizes the shape of the detection volume, τ is the lagtime and τ_D is the diffusion time or the average lateral transit time of a molecule of the fluorophore. Including the contribution of the triplet state;[11]

$$G_{total}(t) = G_{triplet}(t) \,.\, G_{3D}(t) \qquad (2.2)$$

$$G_{total}(t) = \frac{1}{N}\,(1+\frac{\tau}{\tau_D})^{-1}\,\left(1+\frac{\tau}{\tau_D * S^2}\right)^{-1/2}\left(1+\frac{D}{1-D}\;e^{-\tau/\tau_{triplet}}\right) \qquad (2.3)$$

Where D is the fraction of molecules residing in the triplet state and $\tau_{triplet}$ is the triplet state relaxation time. The percent of molecular population found in the triplet state is explained in the next chapter.

The development of laser sources and avalanche photodiodes for detection with a confocal microscope minimized the effective volume, further enhancing the signal to noise ratio of FCS. The custom-built FCS experimental setup has been illustrated in figure 2.2. A collimated excitation laser source (Ar^+ or diode) is focused on the sample through a series of optical lenses and a dichroic mirror via an objective with a high numerical aperture. The objective immersion oil has a refractive index of 1.4; therefore there is minimal refraction of light from glass to oil. This preserves the quality of the image and the resolving power. The emitted fluorescence is collected by the same objective and is focused on a pinhole that reduces the background light from outside the focal volume. An Avalanche Photo Diode (APD) in single photon counting mode detects fluorescence emitted from the sample. APDs have high quantum efficiency as compared to photomultiplier

tubes (PMT) and its sensitivity extends into the near infrared region. A counting board stores and processes detected photon counts for FCS measurements. Photon counts are then autocorrelated using a multi-tau algorithm written in Labview software.

2.3 Results and Discussion

Martinez *et. al.*[12] have compared two fluorescence techniques, FCS and fluorescence intensity histograms (IH) under high and low background conditions. Under high background conditions, either of the parameters (FCS or intensity) was insufficient to differentiate between control and apoptotic cells. FCS and IH measurements were combined to explore the dynamic range of cells stained with Calcein-AM. These experiments help in designing new improved conditions for carrying out cell assays and improve sensitivity of measurements.

Figure 2.3 illustrates the dynamic range of cells stained with Calcein-AM expanding to two orders of magnitude when the FCS and IH measurements are combined. The figure depicts an optimum window for FCS analysis and intensity measurements for calcein-AM viability assays. Calcein-AM identifies viable cells that stain calcein-positive, while cells that do not stain (calcein-negative) are considered dead. FCS identifies ramos cells as 100% calcein-positive from a staining concentration of 0.1 – 1 μM below and above which the autocorrelation signal was too low to be determined by the system. For intensity measurements, concentrations below 10 μM calcein-positive cells are smaller in fraction due to decreasing intracellular calcein concentration.

Therefore, combining FCS and intensity histograms gives the range of cell detection for calcein-AM probe that is extended by two orders of magnitude.

2.4 Conclusion

The FCS instrumental setup yields both autocorrelation function and intensity histogram with a greater signal to noise ratio and low background. The autocorrelation function can further be employed to calculate diffusion times and molecular brightness of extant fluorescent probes. FCS and intensity measurements can be performed simultaneously using the photon counting software to determine the limit of detection and dynamic range of cell detection.

2.5 References

1. G. Seisenberger, M. U. Ried, T. Endress, H. Buning, M. Hallek, and C. Brauchle, *Science*, 2001, 294 (5548), 1929–1932.

2. W. E. Moerner, E. J. Peterman, H. Sosa, S. Brasselet, R. M. Dickson, S. Kummer, R. Sakowicz, and L. S. B. Goldstein, *Biophysical Journal*, 1999, 76 (1), A20–A20.

3. Y. Sako, S. Minoghchi, and T. Yanagida, *Nat Cell Biol*, 2000, 2 (3), 168–172.

4. G. J. Schutz, M. Sonnleitner, P. Hinterdorfer, and H. Schindler, *Mol Membr Biol*, 2000, 17 (1), 17–29.

5. G. S. Harms, L. Cognet, P. H. M. Lommerse, G. A. Blab, and T. Schmidt. *Biophysical Journal*, 2001, 80 (5), 2396–2408.

6. J. Deich, E. M. Judd, H. H. McAdams, and W. E. Moerner, *Proceedings of the National Academy of Sciences of the United States of America* 2004, 101 (45), 15921–15926.

7. D. Magde, W. W. Webb, and E. Elson, *Phys. Rev. Lett.*, 1972, 29 (11), 705.

8. D. Magde, E. L. Elson, and W. W. Webb, *Biopolymers*, 1974, 13 (1), 29–61.

9. E. L. Elson and D. Magde. *Biopolymers*, 1974, 13 (1), 1–27.

10. S. A. Kim, K. G. Heinze and P. Schwille, *Nature Methods*, 2007, 4, 963-973.

11. S. Tanaka, *Soft Matter*, 2012, 8, 8936-8943.

12. M. M. Quiroz, M. Dong, D. Iyer, M. F. Mayer and D. Pappas, Under Review, 2013.

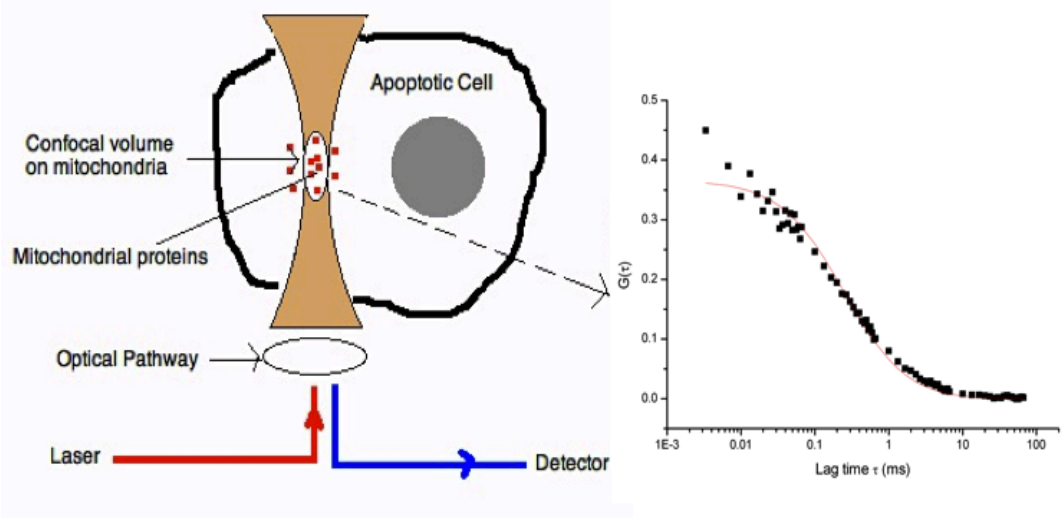

Figure 2.1: Concept of FCS measurements in single cell to study mitochondrial proteins release dynamics in Ramos cells showing a typical autocorrelation curve of a freely diffusing dye molecule. The mitochondrial proteins are labeled with the MitoTracker Deep Red probe and the dye release in an apoptotic cell is assayed indirectly using the mitochondrial assay. When the dye is released into the cytosol, the autocorrelation function changes as dye intensity decreases.

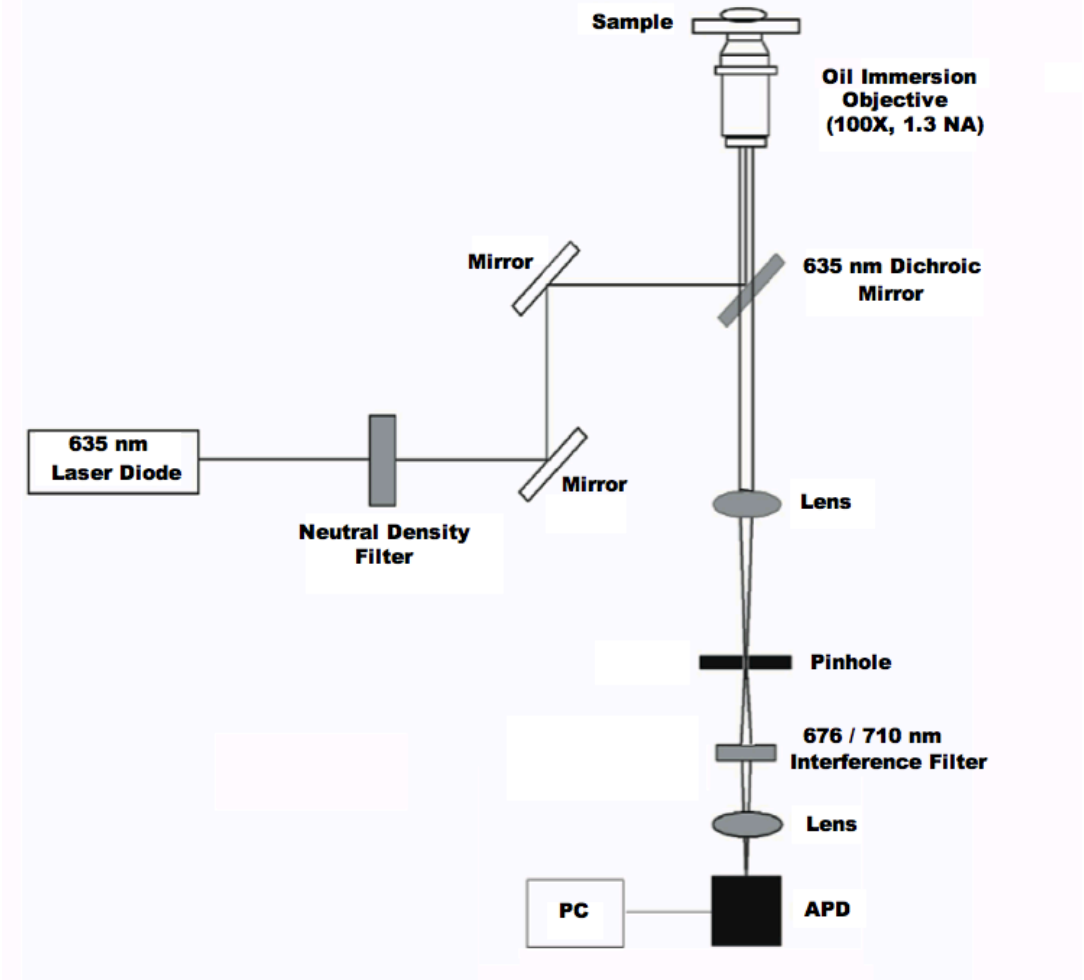

Figure 2.2: Schematic of the custom-built instrumental setup for single molecule detection. A 635 nm diode laser is incident on the sample after passing through a neutral density filter to control the output power. An oil immersion objective (100X, 1.3 NA) is used to focus the light into the cell. The fluorescence emitted by the sample is collected by the same objective, which then passes through an interference filter and a pinhole to spectrally and spatially filter the light, respectively. Photons are then detected by an Avalanche Photo Diode (APD) in single photon counting mode. The single photon counts collected by the APD result into an autocorrelated signal and photon counting histogram on a Personal Computer (PC) with Lab View Software.

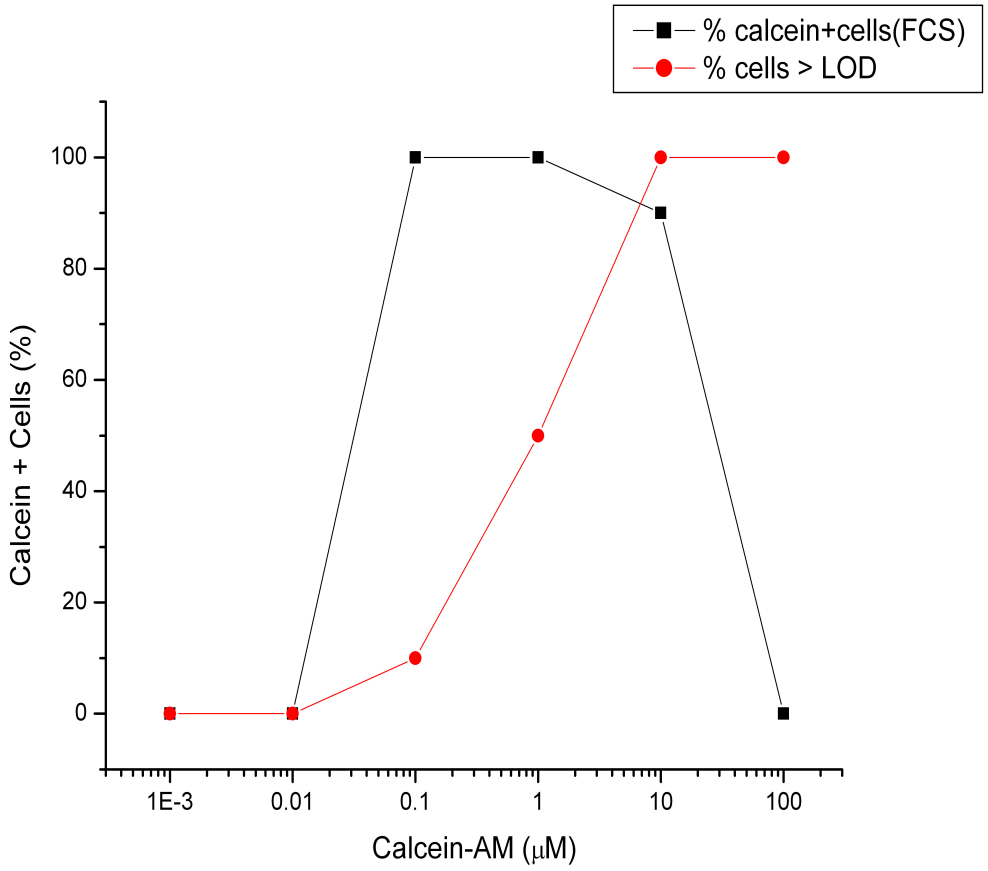

Figure 2.3: Identification of cells as positive or negative for an intracellular probe.[12] The graph shows the percentage of cells identified as positively stained with calcein as a function of calcein concentration. The staining concentration of cells is not the intramolecular calcein concentration. The red circles show the increase in the intensity above the limit of detection (LOD) until the high background range is reached. The black squares shows that FCS continues to identify cells as positive for calcein in the concentration range from 0.1 to 10 μM Calcein-AM. FCS and intensity histograms are generated for individual Ramos cell simultaneously. These measurements can be employed to extend the dynamic range of cell viability identification.

CHAPTER 3

HIGH TEMPORAL RESOLUTION FLUORESCENCE MEASUREMENTS OF A MITOCHONDRIAL DYE FOR DETECTION OF EARLY STAGE APOPTOSIS

Divya Iyer, Rachel D. Ray, Dimitri Pappas*
Published in *Analyst*, 2013,138, 4892-4897

3.1 Introduction

The detection of apoptotic events plays an important role in diagnosing and treating several diseases such as cancer, heart diseases, muscular dystrophy, aging, etc.[1-4] Most chemotherapeutic agents mediate their effects by induction of apoptosis in cancer cells.[5] The early detection and characterization of individual cells is an important clinical finding to initiate early treatments for cancer. A highly sensitive and high throughput single cell detection technique would be capable of diagnosing the earliest stages of diseases in a cell population and help track patient response to treatments. Therefore, there is a clear need to develop technologies supporting single cell analysis with high temporal resolution. Since mitochondria-driven apoptosis has been the main target for many drugs,[6] this mechanism has been explored by various analytical techniques.

Early stages of apoptosis can be detected by monitoring the mitochondrial dysfunction caused by the depolarization of the mitochondrial membrane.[7] Mitochondrial Outer Membrane Permeabilization (MOMP) is the major cause of the release of mitochondrial proteins that are situated in the inter-membrane space.[8-9] The spatial and temporal dynamics of the mitochondrial membrane permeability have been reported to fluctuate due to

the differential release dynamics of these proteins.[7] Therefore, there has been a continuing need for apoptosis assays that can show a steady response of the mitochondria-driven process at early stages.

Depolarization of the mitochondrial membrane post apoptosis induction have been measured using several fluorophores in the past, such as 3,3'-dihexyloxacarbocyanine iodide (DiOC6),[10] JC-1,[11] MitoTracker Red (CMX-Ros),[12] and many more.[13] Protein release from mitochondria has been reported to happen through opening of the mitochondrial permeability transition pore (MPTP) located in between the inner and outer membranes.[14] JC-1 assays are commonly employed for measuring mitochondrial membrane potentials.[11] However, J-aggregate formation in the JC-1 assay need a high $\Delta\Psi$ and are not suitable for fixed samples.[19] Our technique measures changes in the mitochondrial membrane at times before it is reasonably depolarized for J-aggregate formation.

Most of the standard apoptotic assays[20-25] lack sufficient temporal resolution to study apoptosis in real time in living cells. In order to elucidate earliest stages of apoptosis completely, rapid assays with high temporal resolution are required to minimize the time between induction and detection.[26-27] Release of cytochrome c in single cells can be completed within few minutes,[28] thus it is necessary to be able to obtain measurements with high temporal resolution. Our method measures rapid changes in the mitochondria by potent apoptosis inducing drugs with a temporal resolution of five minutes.

Although the change in membrane potentials can be measured by flow cytometry,[15] and plate readers,[31,32] these methods is incapable of collecting single cell response repeatedly within a short time frame. Moreover, a wash step is required to remove the excess dye that can contribute to overlapping of small signals that can otherwise be easily detected in the absence of high background.[33] Ultrasensitive Confocal Fluorescence Microscopy (UCFM) is an ideal analytical technique to study internal dynamics of living cells at sub-nanomolar concentrations with sub-microsecond temporal resolution[34]. Table 1 illustrates a comparison of some most commonly employed instruments and their specifications. In addition to detection of concealed events or events overlapped by bulk signal, UCFM also has the capability to be integrated to microfluidic devices.[35]

In the present study, the accumulation of MitoTracker Deep Red apoptosis probe in the mitochondria of Ramos cells was monitored after apoptosis induction. The temporal resolution and release kinetics of the red probe inside the cellular mitochondria have been explored and the dye release was observed to occur within 5 minutes after staurosporine induction. Induction kinetics varied with the dose of staurosporine. The high temporal resolution, simplicity, capability of integration with microfluidic devices and rapid analysis make our technique amenable to facilitate earliest detection of apoptotic events in living cells.

3.2 Experimental

Materials and Reagents. The mitochondrion-selective probe MitoTracker Deep Red FM (MTDR) and sterile Phosphate-Buffered Saline (PBS, pH = 7.4) were purchased from Invitrogen. Bovine Serum Albumin (BSA) was purchased from Sigma- Aldrich. The apoptosis inducing agents, staurosporine and anti-human CD95 (APO-1/Fas) were purchased from Calbiochem and eBioscience, respectively. Annexin V-FITC apoptosis detection kit that includes Annexin V-FITC conjugate probe and Propidium Iodide (PI) was purchased from BioVision and the Annexin-binding buffer (1X) was purchased from SouthernBiotech.

Cells and Cell Culture. The human cell line Ramos (B lymphocyte) was obtained from American Type Culture Collection (ATCC, Rockville, MD). The cells were sub-cultured at 37° C and 5% CO_2 in RPMI 1640 growth medium (Hyclone) with 10% Fetal Bovine Serum (Hyclone) and 20 mL/L antibiotic (penicillin-streptomycin by Sigma-Aldrich) solution twice a week.

Induction of Apoptosis by Staurosporine. Prior to induction of apoptosis using staurosporine, the cells were centrifuged (4500 rpm for 3 minutes) and re-suspended in two petri dishes (control + sample) in growth medium at a density of ~3 x 10^6 cells/mL measured by a haemocytometer. MitoTracker Deep Red probe was dissolved in dimethylsulfoxide (DMSO) to prepare a 1 mM stock solution and was stored at -4° C. The cells in both petri dishes were stained with 0.1 μM MitoTracker Deep Red probe by incubating the cells in the dark at 37° C for 40 minutes. Apoptosis in the sample petri dish was induced with 4 μM staurosporine. 200 μL of the cell suspension was

drawn from each of the petri dish (sample and control) at each time interval, centrifuged, re-suspended in PBS, and was assayed immediately by microscopy and flow cytometry from 0th minute to 4 hours. Both control and sample measurements were recorded at 5 or 15-minute intervals, depending on the experiment.

Induction of Apoptosis by Anti-CD95. The same procedure as that of staurosporine induction described above was carried out for apoptosis induction by the extrinsic pathway using 0.8 and 1.6 μg/mL of anti-CD95 antibody instead of staurosporine. Control and sample measurements were obtained every hour for a total of 4-hours.

The cell culturing procedures, cell staining protocols and safety considerations followed during the experiments confirms to existing lab protocols.[36]

Microscopy Imaging. Fluorescence imaging was carried out using an inverted microscope (IX-71, Olympus). A metal halide lamp was used for fluorescence excitation using filters appropriate for MitoTracker Deep Red excitation and emission. The images were acquired using a 0.3 NA 10X objective with a 12-bit CCD camera (Orca-285, Hamamatsu). The images were then processed using ImageJ (v. 1.41, National Institutes of Heath) for intensity measurements.

Ultrasensitive Confocal Fluorescence Microscopy (UCFM) Measurements. A custom-built single molecule detection system was employed to acquire ultrasensitive fluorescence intensity measurements. The instrumental setup has been described in details by Dong *et al.*[37] A red diode laser (635 nm, Edmund Optics) was incident on the back port of a microscope

base (IX51, Olympus) through a mirror periscope.[38] A handheld power meter (Laser Check, Edmund Optics) was used to measure the laser power before the cells were exposed to the laser beam. The sample consisted of a 30 μL droplet of Ramos cells (10^5–10^6 cells/mL) in PBS placed on a 150 μm glass coverslip. An oil-immersion objective (100X, 1.3 NA, Olympus) was used to focus the laser beam inside individual cells. One cell was aligned within the confocal volume at a given time, and in this manner five cells were serially illuminated. One spot in each cell was measured for 10 seconds and the time lag between subsequent cell measurements was around 5 seconds. In our measurements, the placement of the laser beam focal point in the cell did not statistically influence fluorescence signals. Fluorescence from MitoTracker Deep Red (Ex: 644 nm, Em: 665 nm) was collected by the objective, passed through the dichroic mirror and then via a 676 nm (Omega Optics) interference filter. Finally, the fluorescence intensity was detected by a single-photon avalanche photodiode (SPCM-AQR 14 Single Photon Counting Module, Perkin-Elmer) via an aspheric lens (Newport).[39] The integration time of the avalanche photodiode was 1 ms.

Immediately after the addition of the sample/control drop on the coverslip, the cells were exposed to 50-90 μW of laser beam and fluorescent counts were acquired with a continuous exposure of cells to the laser beam for 10 s. No significant photo bleaching was observed during data collection. Data was monitored and acquired simultaneously using a Labview program (version 8, National Instruments). A photon counting histogram was obtained for every measurement and then imported to Origin for analysis. The median

fluorescence intensity values obtained for five cells were averaged and plotted as a function of time.

Flow Cytometry. Suspensions of stained cells, with and without apoptosis inducers, were analyzed using FACSCalibur flow cytometer (Becton–Dickinson). The apoptosis induction by both mitochondrial pathway and extrinsic pathway was verified. Two molecular probes were employed for verification of apoptotic cell population induced by anti-CD95.

Staining with MitoTracker Deep Red probe. Cell samples (500 μL from each petri dish) treated with 1.6 μg/mL of anti-CD95 and control cells were centrifuged, re-suspended in PBS and analyzed by forward scatter (FSC), side scatter (SSC) and MitoTracker Deep Red fluorescence (FL 4, ~661/16 nm long pass filter) using CellQuest software every hour for four hours duration. *Staining with Annexin V-FITC/PI:* Cell samples treated with 1.6 μg/mL as mentioned above were centrifuged and re-suspended in 200 μL of 1X Annexin binding buffer. The cells in this buffer were treated with 2 μL Annexin V-FITC probe and 2 μL PI (50 μg/mL). The sample was incubated at room temperature in dark for 5 minutes before re-suspending the cells in PBS for analysis by flow cytometer. Cells were characterized by forward and side scatter (scatter plot) as well as the fluorescence of Annexin V-FITC and PI. The scatter plots were subjected to quadrant analysis to discriminate between apoptotic cells, live cells and dead cells.

3.3 Results and Discussion

Staurosporine Induction of Ramos Cells. In order to observe the change in fluorescence intensity of apoptotic cells, white light and red fluorescence images were acquired every 15 minutes over 2 hours for controls and samples using light microscopy. The decrease in intensity for the sample cells as compared to the control cells (Figure 3.1) indicates that apoptosis was induced in the cells with acceptable spatial resolution. However, the temporal resolution of 15 minutes and the sensitivity of detection on an inverted microscope with a halide lamp were insufficient to observe fast changes in cell fluorescence (Figure 3.2). Mitra *et. al.*[40] have demonstrated use of fluorescent dyes for obtaining high resolution time lapse images of mitochondria but it lacks the high sensitivity offered by a confocal system. On the other hand, for high spatial resolution, cells require labeling with comparatively higher concentration of probe (<100 nM). At these concentrations, there is a risk of over-staining that may increase the probability of labeling other cell organelles. UCFM is a very sensitive technique due to extremely low concentration of fluorescent molecules needed for measurement using a single photon detecting system. Therefore, UCFM was employed for rapid intensity measurements in the mitochondria with sensitivity good enough to show considerable change in magnitude over a short time period.

Temporal Resolution of MTDR by UCFM Measurements: The intensity decline observed by microscopy imaging was confirmed by flow cytometry. Scatter plots and histograms were analyzed to monitor the change in MTDR

intensity over time. MTDR fluorescence of non-apoptotic (control) cells did not change over time and showed higher intensity as compared to the induced cell population (Figure 3.3). This observation agrees with the MTDR fluorescence data obtained by F.Martinez-Pastor *et al*.[41] on apoptotic spermatozoa. The steady decrease in fluorescence intensity of apoptotic cells over an hour gave rise to the need to monitor the intensity change at the shortest time interval possible. To achieve this goal, we employed UCFM methods to detect small changes in MTDR intensity.

To indirectly monitor the rapid release of proteins from the mitochondria post induction, fluorescence measurements were acquired by focusing the red laser beam inside individual cells at five-minute intervals. Data from five random cells were collected as photon counting histograms and median intensity (determined by Gaussian fit) were averaged. Five cells were chosen for each measurement because it was the fastest way possible to collect data from five static cells during each measurement post cell workup, which includes washing and centrifuging the aliquots before each measurement. For this analysis, the wash step was found to be critical to increasing sensitivity.

Another barrier in fluorescent measurements is autofluorescence from green fluorescent molecules present in cells such as NADH and $FADH_2$ that lowers the S/N ratio; in turn affecting spatial resolution.[29] Most of the commercial dyes that are excited at 488 nm overlap with the autofluorescence spectral region (>500 nm) that interferes with the dye fluorescence

considerably. The use of deep red probe eliminates the possibility of cellular autofluorescence interference and increases the signal to noise ratio.

Figure 3.4 demonstrates the steady, exponential decrease in photon-counts with time with a 1/e time (τ) of ~28 minutes. Control cells show stable fluorescence intensity over the measurement period (Figure 3.5). The intensity difference between the apoptotic and control cells are statistically significant at each time interval, based on t-tests at 95% confidence interval. Based on these results, we propose that protein release from the mitochondria is a near-instantaneous process that initiates within few minutes post induction by the intrinsic pathway.

We also carried out a staurosporine dose-dependent study to verify that the rapid decrease in MTDR fluorescence was due to apoptosis induction (Figure 4.6). Cells induced with 0.4 μM staurosporine (10x staurosporine dilution) showed a slower rate of fluorescence intensity decay with a 1/e time of ~38 minutes as compared to the 4 μM dose (Figure 3.6). However, a 100x dilution of the drug doses (0.04 μM) did not show significant changes between control and sample cells over the experiment duration (Figure 3.6b). Our methods are therefore capable of determining differences in apoptosis kinetics based on the target compound dose. The 1/e (t) decay time for fluorescence intensity (Figure 3.7) follows a dose-response curve, with decreasing τ values with increasing staurosporine concentration. Staurosporine is a potent apoptosis inducer, but this approach can be used with less potent compounds as well, elucidating the earliest stages of programmed cell death. Cell response can therefore be identified earlier than

extant assays, and the same cell can be tracked over time to observe later cell response as well. This methodology can therefore be used to probe the temporal dynamics of an anti-cancer drug, and can be applied to compliment methods such as flow cytometry that are used to assay viability and toxicity at later time points after drug administration.

Receptor-Mediated Apoptosis Measurements. To ensure that the intrinsic apoptosis pathway was being triggered with staurosporine, we used our methods with a receptor-mediated apoptosis inducer. There is a limit to the number of Fas receptors present on a cell membrane; hence the time of induction through the extrinsic mechanism can be longer as compared to the mitochondrial pathway. Since receptor-mediated apoptosis does not directly involve mitochondria, we did not anticipate a rapid change in MTDR fluorescence after the induction event. However, when the receptor-mediated pathway also triggers mitochondrial apoptosis, there is a lag between apoptosis induction and a decrease in MTDR fluorescence. Almost no significant intensity decline was observed between the apoptotic and control cells (Figure 3.8). To confirm the results obtained by UCFM, cells were stained with MTDR and induced with anti-CD95 for monitoring using flow cytometry. Figure 3.9 shows no decline in the MTDR fluorescence for apoptotic and non-apoptotic Ramos cells. These results prove that the mitochondrial inter-membrane proteins are not involved in the extrinsic apoptotic pathway of Ramos cells using anti-CD95 antibodies.

To ensure that apoptosis is still being induced by anti-CD95, an Annexin V-FITC / PI assay was carried out using flow cytometry to study

downstream apoptosis markers. Induction of apoptosis was observed from the third hour, which showed ~8% apoptotic cells (staining Annexin+/PI-), ~78% viable cells (Annexin-/PI-) and ~14% necrotic cells (Annexin+/PI+) (Figure 4.10). Similarly, the control measured at 3h had ~90% viable cells, ~1% apoptotic cells and ~9% necrotic cells (Figure 3.10b). The observations confirm induction of apoptosis in Ramos cells by anti-CD95 via the extrinsic pathway, and that the intrinsic pathway is not triggered during receptor mediated apoptosis in this cell line.

Release of Mitochondrial Contents During Apoptosis: During the intrinsic apoptosis pathway, release of mitochondrial contents is a complex process. UCFM measurements can be conducted alongside Fluorescence Correlation Spectroscopy (FCS) measurements using the same dataset. We observed anomalous diffusion curves for the MTDR probe by FCS that failed to fit standard 3D cytosol diffusion models. The FCS measurements of anomalous diffusion confirmed the complex release dynamics of the mitochondrial proteins in apoptotic cells (Figure 3.11). Further investigations are required to study the spatial variations and the molecular diffusion behavior of MTDR. The application of FCS to subcellular organelles such as the mitochondria in this case, can be challenging due to two reasons. First, the fluctuating release dynamics of the mitochondrial proteins do not always provide the necessary conditions essential for obtaining autocorrelation. Second, parameters that cause fluorescence fluctuations in apoptotic inducers need to be time-independent to attain local equilibrium conditions necessary for correlation.[42] Recent studies by Lingao Ruan *et. al.*[43] show detection of drug

induced apoptosis by FCS based on DNA fragmentation during the process. A modified version of FCS has been explored for a mixture of nanoparticles with similar diffusion coefficients to analyze the binding of TMRE in isolated mitochondria.[44] However, combining MTDR staining with FCS to explore single molecule diffusion in live cells is not yet explored.

Figure 3.11 represents anomalous diffusion of mitochondrial proteins in live apoptotic cells possibly due to highly disordered diffusion of molecules from a moving mitochondrion in a static cell. The curve shows a distinct shoulder, which accounts for intersystem crossing of MTDR to a triplet blinking state where, the fluorophore is temporarily unable to emit photons.

The FCS 3D Diffusion Model is given by;[34]

$$G_{3D}(\tau) = \frac{1}{N}\left(1+\frac{\tau}{\tau_D}\right)^{-1}\left(1+\frac{\tau}{\tau_D * S^2}\right)^{-1/2} \quad (3.1)$$

Where, $G_{3D}(\tau)$ is the autocorrelation function for a 3D fit, N is the number of molecules in the probe volume, S is the structure parameter that characterizes the shape of the detection volume, τ is the lagtime and τ_D is the diffusion time or the average lateral transit time of a molecule of the fluorophore. Including the contribution of the triplet state;[45]

$$G_{total}(\tau) = G_{triplet}(\tau) \,.\, G_{3D}(\tau) \quad (3.2)$$

$$G_{total}(\tau) = \frac{1}{N}\left(1+\frac{\tau}{\tau_D}\right)^{-1}\left(1+\frac{\tau}{\tau_D * S^2}\right)^{-1/2}\left(1+\frac{D}{1-D}\; e^{-\tau/\tau_{triplet}}\right) \quad (3.3)$$

Where, D is the fraction of particles residing in the triplet state and $\tau_{triplet}$ is the triplet state relaxation time.

In this work, there is a clear fraction of molecules in the triplet state (Figure 3.11).

The triplet fraction observed was approximately 25% of the total molecular population. The diffusion time of MTDR was longer than similarly sized fluorophores observed to freely diffuse through the cytosol.[26] The triplet state relaxation time of 0.04 ms was obtained in these studies. Our future work will be based on trying to identify and interpret the cause of such a diffusion pattern observed in MTDR fluorescence in apoptosis induced cells.

The dynamics of early apoptotic changes by the intrinsic pathway start from intact mitochondrial membrane potential. Depolarization of the membrane potential gives rise to formation of Mitochondrial Permeability Transition Pore (MPTP), followed by release of mitochondrial inter-membrane proteins, and lastly activating caspases leading to cell death. The results of this study agrees with the results found by F.Martinez-Pastor et.al.[40] for early apoptotic changes observed in sperm cells using MTDR fluorescence, assuming the apoptosis in sperm cells partly resemble most of the other cell types. However, we propose that these early apoptotic changes in the mitochondria begin rapidly with the addition of inducing drugs like staurosporine. Commonly used Membrane-potential-dependent dyes such, as Rhodamine 123 and TMRM/TMRE are useful as long as the mitochondrion maintains its negative membrane potential. Tait *et. al*.[23] have demonstrated successful use of TMRE to measure changes in $\Delta\Psi$ in living cells due to its low toxicity. However, TMRE also has a tendency to redistribute itself across the plasma membrane.[24] Once the process of cell death becomes irreversible after apoptosis induction, the plasma membrane lysis begins within 30 minutes[25] and therefore fluorescent measurements using plasma membrane

potential sensitive dyes like Rhodamine 123, TMRM/TMRE can give spurious results after 30 mins. Therefore, it is advantageous to use MTDR in multiple labeling experiments for steady monitoring of intensities for longer time periods. The high temporal resolution and simplicity of our methods allows new insights into the mechanisms of early stage apoptosis.

3.4 Conclusion

In this study, we employed UCFM for measurements with high temporal resolution, which facilitated rapid time based analyses of the earliest stage of apoptosis. We validated our UCFM assay and instrumental response by comparing the results with other commonly used techniques such as flow cytometry and fluorescence microscopy. The five-minute temporal resolution enabled us to observe near-instantaneous release of mitochondrial contents during apoptosis induction. The kinetics of mitochondrial release followed a dose-dependent response, even though the process started rapidly. In the case of receptor-mediated apoptosis, our method can observe if mitochondrial release occurs, although a lag between induction and detection is expected in these cases. When Ramos cells were used, the receptor mediated pathway did not trigger mitochondrial-driven apoptosis.

We have developed a unique high-resolution assay to study the earliest stages of apoptosis in the intrinsic pathway using a novel analytical tool. The diffusion of mitochondrial proteins in apoptotic cells occurs rapidly after induction and therefore a high temporal resolution technique is important to monitor these early biological changes in cells non-invasively. Our future

efforts will be focused on increasing cell throughput by automation of cell analysis.

3.5 Acknowledgment

R.D. Ray acknowledges support from the Undergraduate Research Fellowship from Texas Tech University. This work was supported by grants from the Robert A. Welch Foundation (Grant D-1667) and the National Institutes of Health (Grants RR025782 and GM103550).

3.6 References

1 O. Yoshinori, L. Zhonglian and S. Masa-Ai, *J. Hisochem. Cytochem*., 2003, 38, 275–340.

2 C. Gill, R. Mestril and A. Samali, *FASEB J*., 2002, 16, 135–146.

3 E. E. Dupont-Versteegden, *J. Appl. Physiol*., 1994, 77, 1736-1741.

4 B. Fadeel and S. Orrenius, *J. Intern. Med*., 2005, 258, 479-517.

5 K. M. Debatin, D. Poncet and G. Kroemer, *Oncogene*, 2002, 21, 8786-803.

6 M. M. Martinez, R. D. Reif and D. Pappas, *Anal. Methods*, 2010, 2, 996–1004.

7 P. D. Bhola, A. L. Mattheyses and S. M. Simon, *Biophysical Journal*, 2009, 97, 2222-2231.

8 D. Wlodkowic, W. Telford, J. Skommer and Z. Darzynkiewicz, *Methods Cell Biol*., 2011, 103, 55-98.

9 C. Munoz-Pinedo, A. Guio-Carrio, J. C. Goldstein, P. Fitzgerald, D. D. Newmeyer and D. R. Green, *PNAS*, 2006, 103, 11573–11578.

10 P. X. Petit, J. E. O-Connor, D. Grunwald and S. C. Brown, *Eur. J. Biochem.*, 1990, 194, 389-397.

11 C. A. Ceccarelli, and A. Massini, *Exp. Cell Res.*, 1996, 222, 84-94.

12 M. Poot, Y. Z. Zhang, J. A. Krämer, K. S. Wells, L. J. Jones, D. K. Hanzel, A. G. Lugade, V. L. Singer and R. P. Haugland, *J. Histochem. Cytochem.*, 1996, 44, 1363-1372.

13 K. Gilmore and M. Wilson, *Cytometry*, 1999, 36, 355-358.

14 N. G. Machado, M. G. Alves, R. A. Carvalho and P. J. Oliveira, *Cardiovasc. Toxicol.*, 2009, 9, 211–227.

15 X. Xue, Y. Song, Q. Zhang, Y. Wu, Z. Guo-zhang, P. C. Wang, Y. Zhao, Y. X. Jia, X. Zhang and X. J. Liang, *Mol. Pharmaceutics*, 2012, 9, 634-644.

16 L. Bouchier-Hayes, C. Munoz-Pinedo, C. Connell and D. R. Green, *Methods*, 2008, 44, 222-228.

17 S. Roy and G. Hajnoczky, *Methods*, 2008, 46, 213-223.

18 S. W. Perry, J. P. Norman, J. Barbieri, E. B. Brown and A. H. Gelbard, *Biotechniques*, 2011, 50, 98-115.

19 A. Cossarizza and S. Salvioli, *Purdue Cytometry CD-ROM series.*, 4, Retrieved from www.cyto.purdue.edu/archive/flowcyt/research/cytotech.htm

20 J. C. Goldstein, N. J. Waterhouse, P. Juin G. I. Evan and D. R. Green, *Nat. Cell Biol.*, 2000, 2, 156–162.

21 N. J. Waterhouse, J. C. Goldstein, O. Ahsen, M. Schuler, D. D. Newmeyer and D. R. Green, *J. Cell Biol.*, 2001, 153, 319–328.

22 E. Gottlieb, S. M. Armour, M. H. Harris and C. B. Thompson, *Cell Death Differ.*, 2003, 10, 709.

23 S. W. G. Tait, L. Bouchier-Hayes, A. Oberst, C. Connel and D. R. Green, *Apoptosis*, 2009, 559, 33-48.

24 A. Wong and G. A. Cortopassi, *Biochem. Biophy. Res. Commun*., 2002, 298, 750-754.

25 D. G. Nicholls and N. W. Ward, *Mitochondria and excitotoxicity* TINS, 2000, 23, 166-174.

26 M. M. Martinez, R. D. Reif and D. Pappas, *Anal. Bioanal. Chem*., 2010, 396, 1177–1185.

27 P. Li, D. Nijhawan, I. Budihardjo, S. M. Srinivasula, M. Ahmad, E. S. Alnemri and X. Wang, *Cell*., 1997, 91,479–489.

28 J. C. Goldstein, N. J. Waterhouse, P. Juin, G. I. Evan and D. R. Green, *Cell Biol*., 2000, 2, 156–162.

29 B. Chazotte, *Cold Spring Harb. Protoc.,* 2011, 990-992.

30 R. D. Reif, M. M. Martinez and D. Pappas, *Anal. Bioanal. Chem*., 2010, 397, 3387-3396.

31 FLIPR application note, Molecular Devices, Retrieved from http://www.moleculardevices.com/Documents/general-documents/mkt-appnotes/flipr-appnotes/FLIPR_App_Note_mito_membrane_rev_B.pdf

32 FLIPR High Throughput Cellular Screening, Molecular Devices, Retrieved from http://www.moleculardevices.com/Products/Instruments/FLIPR-Systems.html.

33 A. E. Florian, C. K. Lepensky, O. Kwon, M. K. Haynes, L. A. Sklar and A. Zweifach, *J. Biomol. Screen*., 2012, DOI: 10.1177/1087057112466697.

34 S. A. Kim, K. G. Heinze and P. Schwille, *Nature Methods*, 2007, 4, 963-973.

35 D. Pappas, S. M. Burrows and R. D. Reif, *Trends in Analytical Chemistry*, 2007, 26, 884-894.

36 D. Pappas, *Practical Cell Analysis*, 2010, First Edition, Wiley.

37 M. Dong, M. M. Martinez, M. F. Meyer and D. Pappas, *Analyst*, 2012, 137, 2997-3003.

38 Y. Tian and D. Pappas, *Appl. Spectrosc.*, 2010, 64, 324-327.

39 R. D. Reif, M. M. Martinez, K. Wang and D. Pappas, *Anal. Bioanal. Chem.*, 2009, 395, 787–795.

40 K. Mitra and J. Lippincott-Schwartz, *Curr. Protoc. Cell Biol.*, 2010, Chapter 4, 1-21.

41 F. Martínez-Pastor, M. R. Fernández-Santos, E. Olmo, A. E. Domínguez-Rebolledo, M. C. Esteso, V. Montoro and J. J. Garde, *Reprod. Fertil. Dev.*, 2008, 20, 547–556.

42 M. Wachsmuth, W. Waldeck and J. Langowski, *J. Mol. Biol.*, 2000, 298, 677-689.

43 L. Ruan, Z. Xu, T. Lan, J. Wang, H. Liu, C. Li, C. Dong and J. Ren, *Anal. Chem.*, 2012, 84, 7350-7358.

44 I. V. Perevoshchikova; D. B. Zorov and Y. N. Antonenko, *Biochimica et Biophysica Acta-Biomembranes*, 2008, 1778, 10, 2182–2190.

45 S. Tanaka, *Soft Matter*, 2012, 8, 8936-8943.

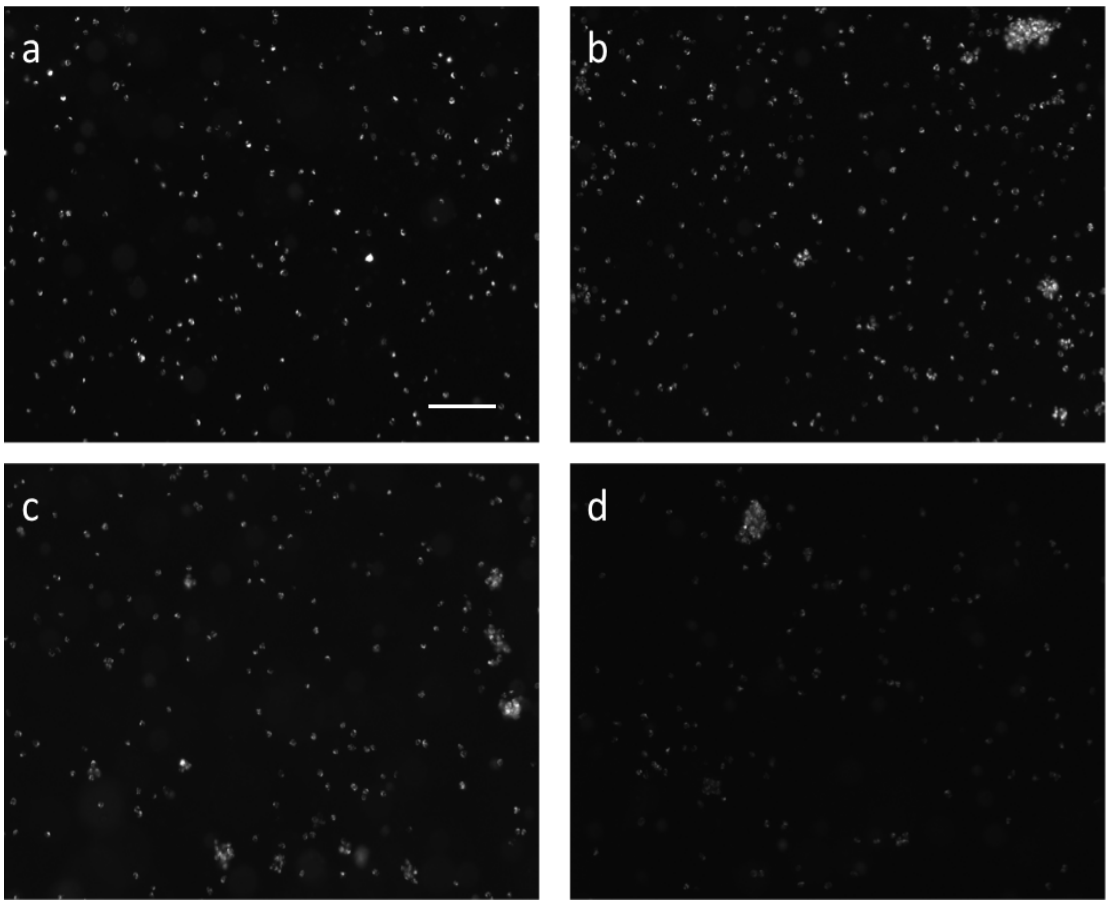

Figure 3.1: Fluorescence images (x10 magnification) of Ramos cells stained with 0.1 μM MitoTracker Deep Red at (a) Control (Avg intensity = 22301, stdev = 2051), (b) 30 minutes (Avg intensity = 17345, stdev = 2119) (c) 45 minutes (Avg intensity = 12897, stdev = 1629) (d) 60 minutes (Avg intensity = 9800, stdev = 1882) after staurosporine induction. The fluorescence intensity was observed to decrease after induction, but the earliest changes were not resolved. The image shows illumination of mitochondria in cells. Scale bar = 100 μm.

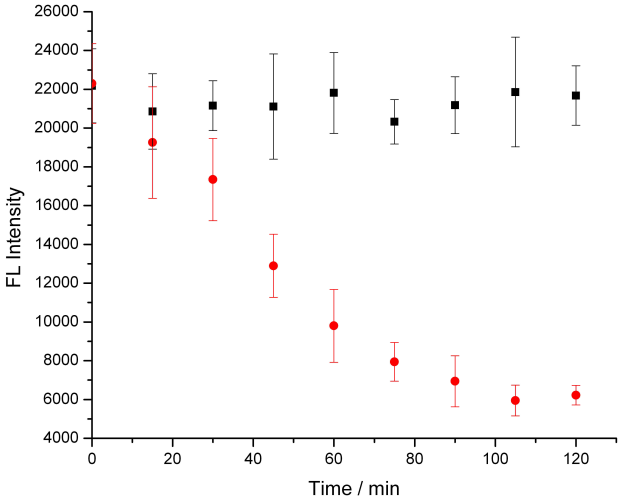

Figure 3.2: The decrease in fluorescence intensity of the sample as a function of time was exponential, whereas the control intensity remained constant for 2 hours. To quantitatively determine the average intensity of apoptotic cells for each image (Figure 3.1), the mean intensity per pixel of ~20 cells was measured using ImageJ. Control cells are represented as black squares and drug induced samples as red circles. All cells were stained with 0.1 μM MitoTracker Deep Red and samples were induced with 4 μM staurosporine.

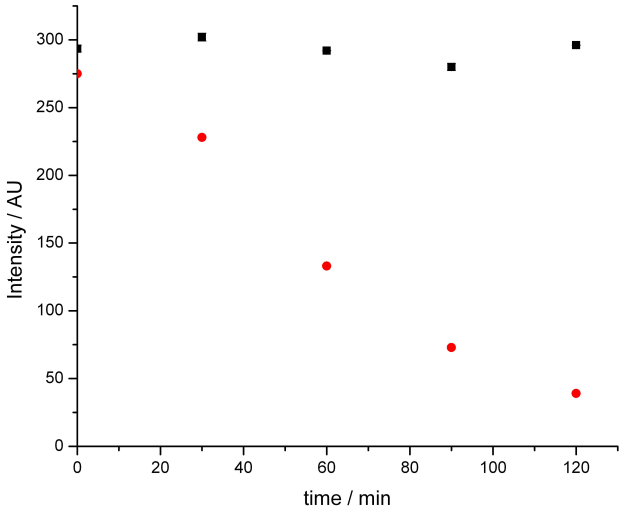

Figure 3.3: MitoTracker Deep Red (MTDR) intensity measurements extracted from flow cytometer FL 4 histogram after inducing with staurosporine as a function of time to confirm the results obtained by microscopy. Control cells are represented as black squares and drug induced samples as red circles. All cells were stained with 0.1 μM MTDR and samples were induced with 4 μM staurosporine. Each data point represents mean of triplicate measurements. Standard error of the mean is too small to be visible.

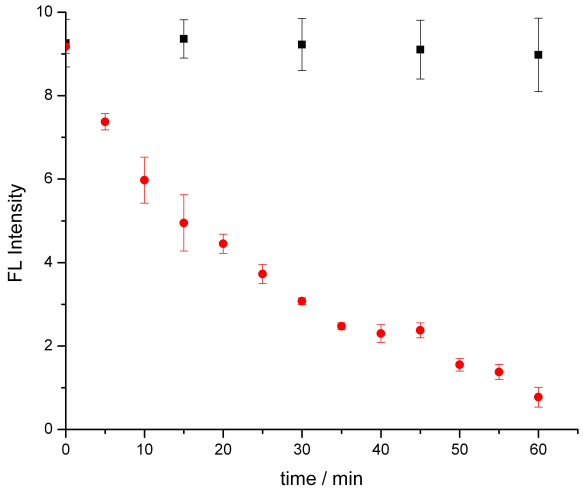

Figure 3.4: Mean MitoTracker Deep Red fluorescence intensity of five Ramos cells at each time interval by ultrasensitive confocal fluorescence microscopy (error bars represent the standard deviation of the mean). Control cells are represented as black squares and drug induced samples as red circles. All cells were stained with 0.1 μM MitoTracker Deep Red and samples were induced with 4 μM staurosporine. The decay in cell fluorescence was measured with a 1/e time = 28 minutes. The five-minute temporal resolution enables early apoptosis events to be analyzed.

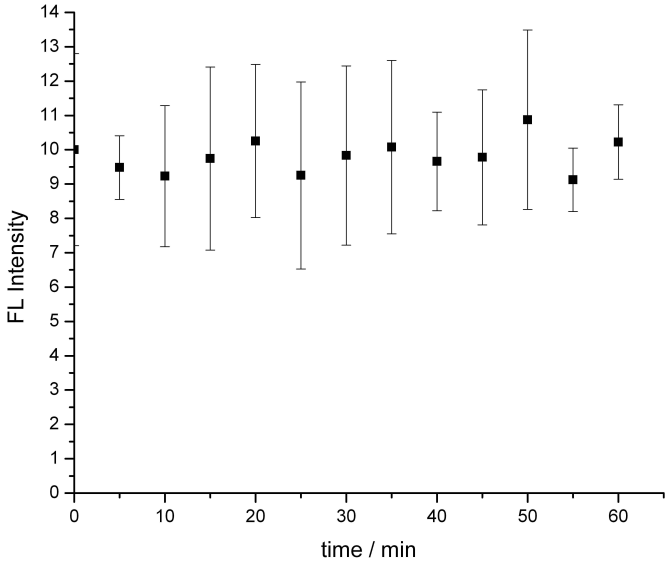

Figure 3.5: Mean of the median MitoTracker Deep Red (MTDR) fluorescence intensity as a function of time for five Ramos cells at each time interval by ultrasensitive confocal microscopy. Control cells are represented as black squares and stained with 0.1 μM MTDR.

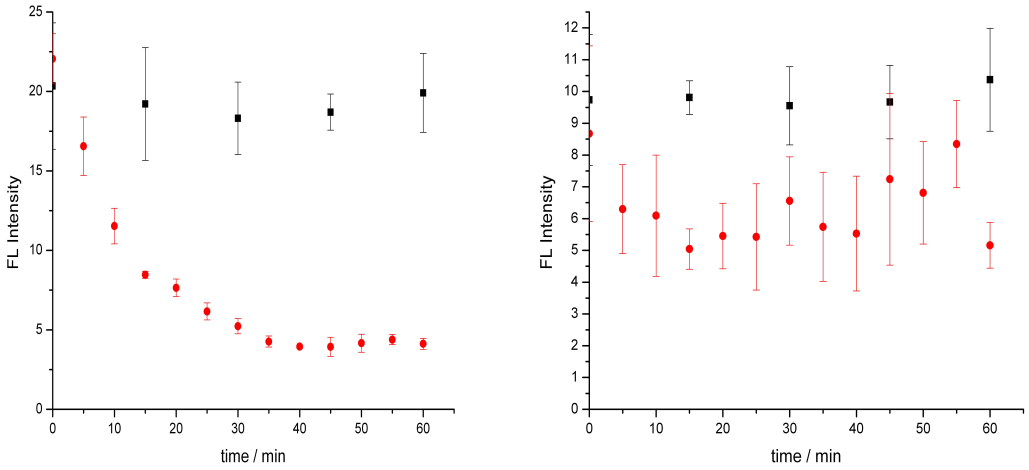

Figure 3.6: Mean MitoTracker Deep Red (MTDR) fluorescence intensity by as a function of time for five Ramos cells at each time interval by ultrasensitive confocal microscopy. Control cells are represented as black squares and drug induced samples as red circles. All cells were stained with 0.1 μM MTDR and samples were induced with (a) 0.4 μM staurosporine or (b) 0.04 μM staurosporine. The 1/e time for the 0.4 μM sample was 38 minutes, and was not measured for the 0.04 μM sample.

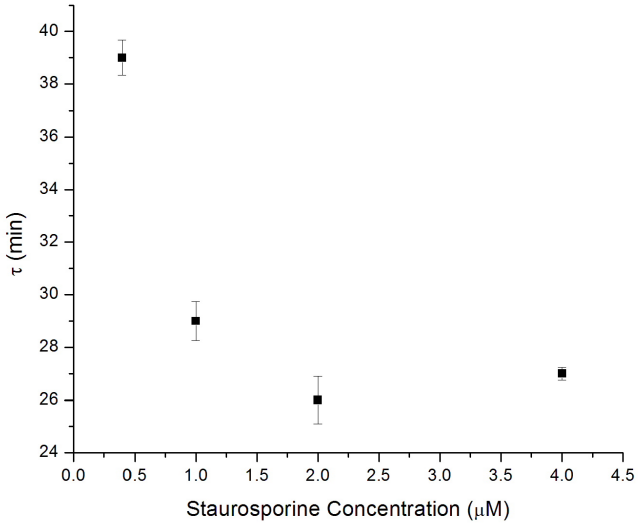

Figure 3.7: The change in decay time (t) with staurosporine concentration. The decay of fluorescence (τ) measured by UCFM occurs more rapidly with increasing staurosporine concentration.

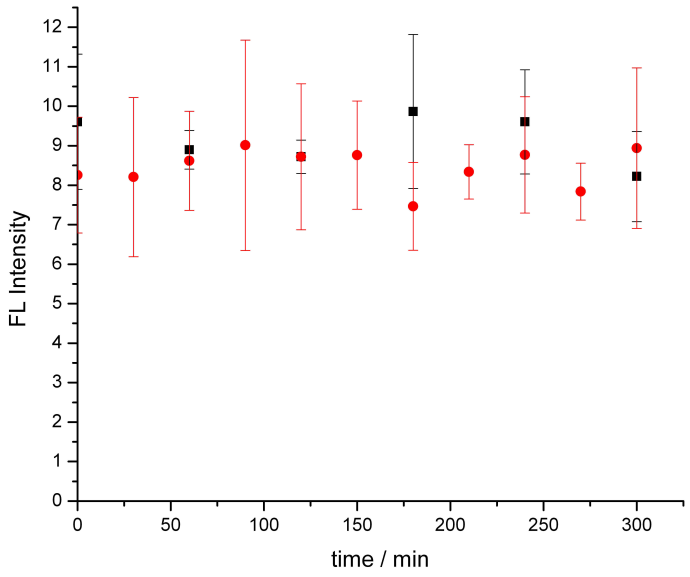

Figure 3.8: Mean of the median MitoTracker Deep Red (MTDR) fluorescence intensity as a function of time for five Ramos cells at each time interval by ultrasensitive confocal microscopy. Control cells are represented as black squares and anti-CD95 induced samples as red circles. All cells were stained with 0.1 μM MTDR and samples were induced with 1.6 μg/ml anti-CD95. No significant change in fluorescence intensity was observed between the sample and control cells.

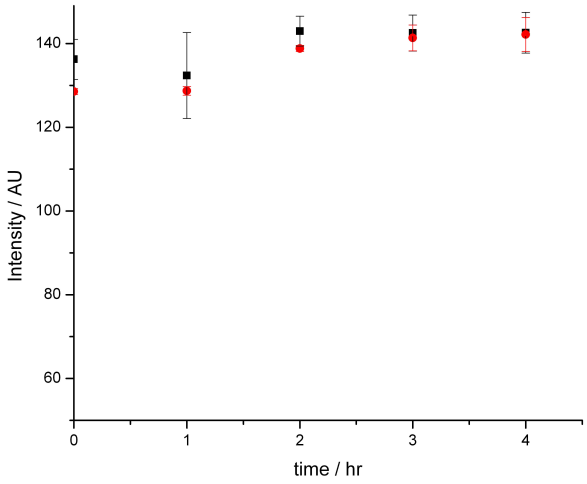

Figure 3.9: MitoTracker Deep Red intensity measurements extracted from flow cytometer FL 4 histogram after inducing with anti-CD95 as a function of time. Control cells are represented as black squares and drug induced samples as red circles. All cells were stained with 0.1 μM MTDR and samples were induced with 1.6 μg/ml anti-CD95. The microscopy results were confirmed by flow cytometry.

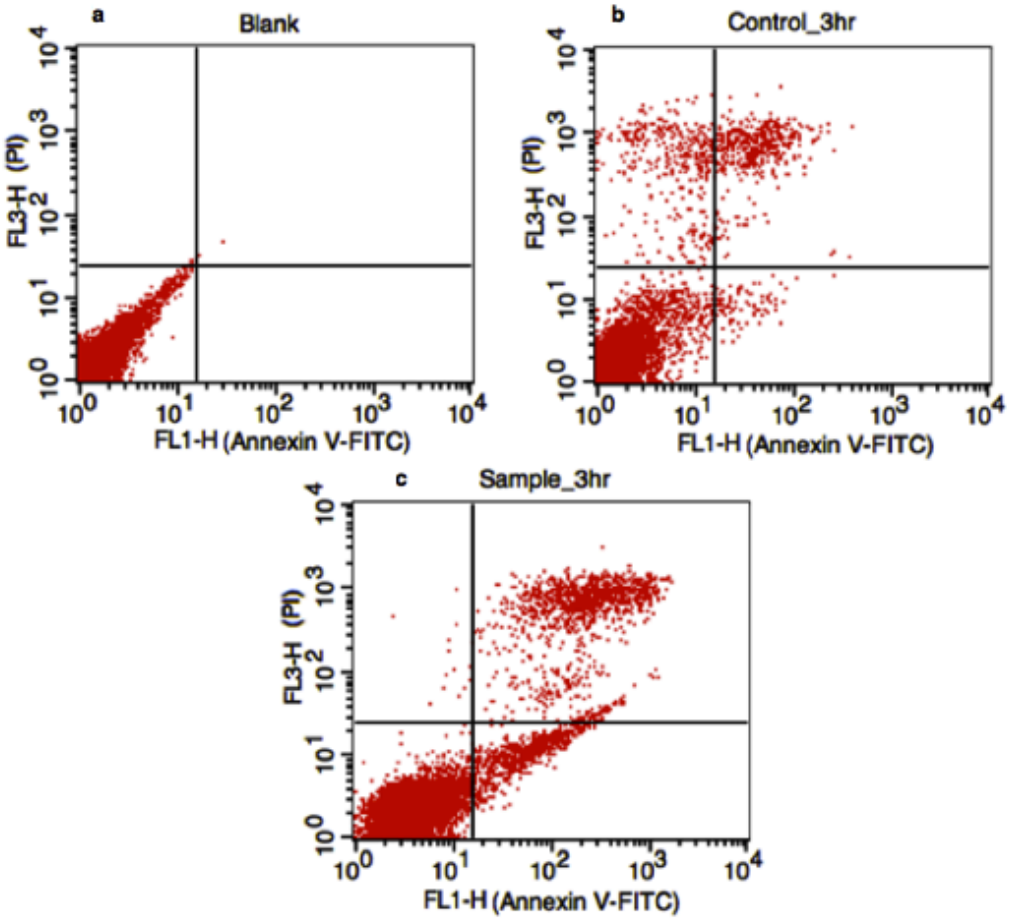

Figure 3.10: Flow cytometry analysis of anti-CD95 induced apoptosis using Annexin V-FITC/PI. Apoptotic cells are located in the lower right quantrant. (a) Control (probe without anti-CD95) and (b) blank (no probe or antibody) showed normal levels of nectrotic and apoptotic cells. However, when receptor mediated apoptosis was initiated, apoptotic cells were observed at 3 hours (c). Given the rapid temporal resolution of our mitochondrial-based assay, it is possible to exclude mitochondrial protein release as a co-mechanism during receptor-mediated apoptosis in Ramos cells.

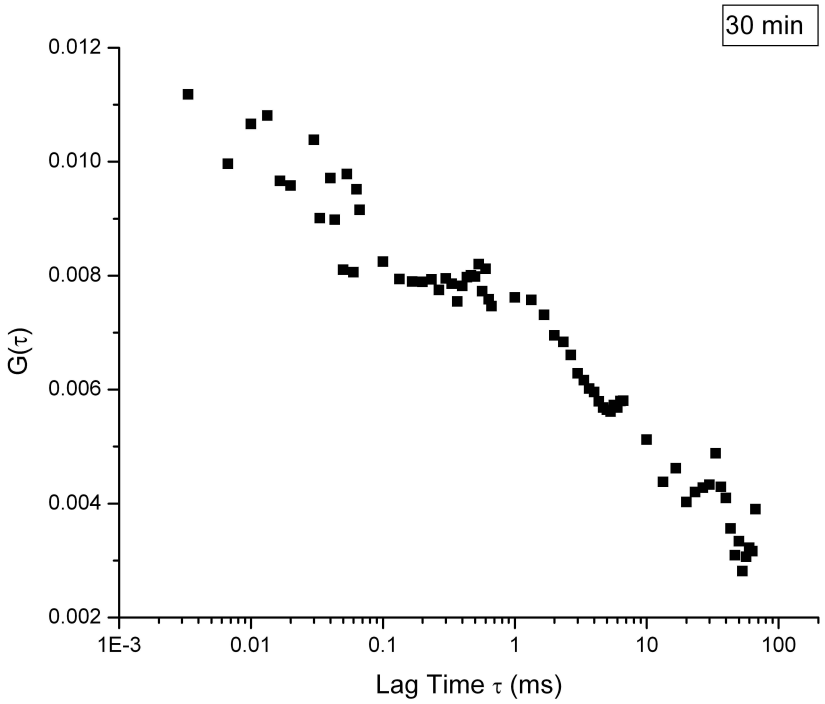

Figure 3.11: Autocorrelation curve of a single cell stained with 0.1 μM MitoTracker Deep Red and induced with 4 μM staurosporine acquired at 30 minutes post induction. The auto-correlation signal was readily detectable over the background. FCS 3D model was a poor fit with a correlation coefficient of 0.73 whereas the FCS Triplet model fit better with a correlation coefficient of 0.96. y

Table 3.1: Comparison of instrumental capabilities commonly used for cellular apoptosis studies.

Instrument Specification	**Flow Cytometry**	**Plate-Based Assays**	**UCFM**
Temporal Resolution	Moderate	High	High
Wash Step Integration	No	No	Yes
Repetitive Single Cell Analysis	No	No	Yes
Integration with Microfluidics	Yes	No	Yes
Subpopulation Analysis	Yes	Yes	Yes
Extended Fluorescence Parameter Measurement*	No	No	Yes
Cost Effectiveness Per Assay	Low	Low	Low

*Extended fluorescence parameters include molecular brightness, molecular diffusion, triplet state fractions, free vs. bound states, etc.

CHAPTER 4

HIGH THROUGHPUT, CONTINUOUS SINGLE-CELL SCREENING USING FCS ON A MICROFLUIDIC PLATFORM

4.1 Introduction

Single cell studies play a vital role in the development of new diagnostic tools for cancer.[1,2] In this study, a single cell Fluorescence Correlation Spectroscopy (FCS) method was applied to High Throughput Screening (HTS). HTS using microfluidic technology needs extensive assay validation due to the high variability induced by PDMS. Cooksey *et. al.*[3] have tested assay robustness and reproducibility in such systems using various illumination sources for cytotoxicity studies on chip. They could detect toxins in the first 60 minutes after induction.

In this study, single cells were assayed for early detection of apoptosis in cells flowing through a microfluidic channel. MitoTracker Deep Red (MTDR) and calcein-AM were used as the fluorogenic probes for this study. There are several routine methods to detect apoptosis in cells such as flow cytometry or light microscopy on cells stained with fluorophore-conjugated annexin V. Other methods include TUNEL (Terminal deoxyribonucleotide transferase-mediated dUTP X Nick end Labeling), DNA ladder assays and enzyme-linked immunosorbent assay (ELISA).[4,5] These methods require cell fixation with extensive sample preparation that decreases the overall temporal resolution of the cellular assay in real time. Moreover, these methods lack the sensitivity required for the early diagnosis of apoptosis. Recent developments have used nanofluidic channels in PDMS to analyze individual isolated

mitochondria to study the Mitochondrial Membrane Permeabilization (MMP) using fluorescence microscopy.[6] However, these techniques do not offer to test the mitochondrial protein release dynamics in cells non-invasively.

A microfluidic based apoptosis assay will be a powerful tool to detect apoptotic cells in a given cell population with analysis speeds greater than comparable methods. Efficient drug development can be carried out using microfluidic systems in a cellular microarray.[7] These experiments require very less volumes of reagents and have been successfully implemented for dose response studies. Since we have already developed a mitochondrial assay to identify apoptotic cells with a temporal resolution of five minutes (chapter 3), the next step is towards high throughput cell scanning using the same spectroscopic method on a microfluidic device. The significance of this work lies in the ability to carry out drug testing with high throughput and high temporal resolution simultaneously.

Single cell analyses have been recognized as powerful tools to understand the population dynamics and to isolate rare cells obtained from pooled measurements. Some of the single cell measurements explored so far include laser micropipettes,[8] single cell capillary electrophoresis,[9] single cell trapping and imaging[10] and single cell mapping.[11] These techniques offer useful information on single cells with high throughput, but lack sufficient sensitivity and cannot be easily automated. Using a flowing stream of cells through a microfluidic channel eliminates sample handling and incorporates automation. Combining the FCS setup with microfluidics offers unparalleled sensitivity and high throughput for early detection of apoptosis in single cells.

The combined capabilities of both techniques can detect rare cancer cells that are resistant to apoptosis induction. A microfluidic apoptosis assay can identify such outlying cells rapidly in a few minutes with a scan rate of ~50 cells per minute. Our method offers high sensitivity detection of apoptosis induction with throughputs comparable to other single cell techniques.

A limitation of the mitochondrial assay discussed earlier (chapter 3) is that it requires manual manipulation of the cell stage and has an overall low throughput with an average rate of 10 cells per minute. The objective of this study is to develop a flowing cell assay using the existing UCFM setup. The assay will scan multiple cells in an automated fashion that would require minimal manual skills and labor. The dimensions of the microfluidic channel are chosen for single cell alignment in order to measure cellular response sequentially. A laser beam interrogates cells using fluorescent assays.

The microfluidic device was constructed from polydimethylsiloxane (PDMS) using soft lithography. PDMS was prepared by mixing the pre-polymer and cross-linking agent in a 10:1 ration (w/w). The PDMS mixture was degassed and poured over a master mold silicon wafer prepared from two-layer spin coating process, using the negative photoresist SU-8 2015 (MicroChem Corp, Newton, MA). The microchannel patterns of standard photolithography were designed using Canvas software and transferred on to chrome masks by electron beam lithography. The PDMS was cured for 45 minutes at 75 °C. A glass microscope was used as the base (substrate) of the PDMS chip.

4.2 Preliminary Studies: To find the lowest acquisition time on FCS

It has been observed that cells undergo shear stress in the microfluidic channels due to acute sandwiching of PDMS layers on glass slides.[12]

Hamon *et. al.*[13] have demonstrated use of open wall micro-chambers for cell based dose response studies to reduce mechanical stress encountered by cells in microfluidic channels. We developed a hydrodynamic focusing chip to streamline the cells flowing into the microfluidic channel and to reduce mechanical stress in cells (Figure 4.1). Hydrodynamic focusing occurs when two opposite streams meet at a cross-junction and flow parallel to each other under laminar conditions. In this case, the two opposite streams consist of a buffer to streamline and focus the cells in the center stream. This microfluidic network provides control over cell residence time in the confocal volume and enables separation of single cells from bulk suspension and provides stability in the cellular flow, thus enabling precise optical analysis of single cells. Residence time is the average amount of time a cell spends in the probe volume, which can be obtained by measuring the time trace base peak width. The average residence time for cells flowing through the hydrodynamic focusing chip was observed to be 2.5 ms. The linear flow rate can be calculated from the linear velocity and volumetric flow rates.

Total channel volume, $V = \pi R^2 L$ where, R is the channel radius and L is the channel length. V is in ηL when L is expressed in μm.

The linear velocity, $v = L/t$ where, t is the residence time of cell in the confocal volume.

Linear flow rate in cm/hr., $u = F/\pi R^2$ where, F is the volumetric flow rate in ml/hr.

The preliminary studies involved linear flow rate optimization of the buffer and cells to produce a stable stream of cells. We then conducted temporal resolution studies to find the shortest acquisition time on FCS for static and flowing cell measurements. Table 4.1 gives a summary of various flow rates employed for the study and their respective Xc value (from PCH), flow time, number of molecules observed in probe volume (N) and the autocorrelation observed. Xc values (median fluorescence intensity) are obtained after the Gaussian fit of the photon counting histograms on Origin software. It was observed that at certain flow rates the autocorrelation curves showed a better FCS fit with the FCS flow model with N reaching unity. This study helps to optimize the flow rates to obtain the ideal autocorrelation function with R square greater than 0.99. Figure 4.2 and 4.3 compares the autocorrelation curves obtained from calcein stained static Ramos cells on FCS for acquisition times ranging from 1 s to 20 s. Under non-flow conditions, autocorrelation was observed with acquisition time as low as 1 s. This proof-of-concept shows high throughput FCS acquisition along with intensity and time trace plots. This test was applied to flowing cells for high throughput cell screening with high sensitivity.

Figure 4.3 compares the FCS information obtained with an FCS acquisition time of 20 s and 1s that are reasonably comparable. Therefore, it is possible to acquire FCS measurements in a time frame as small as 1 s with a cell flow rate of 3 cells per second. We estimate that in faster cases 100s of

cells can be analyzed per minute, yielding single cell data with high sensitivity and throughput. The benefit of this method is that it mimics fluidic flow observed in a flow cytometer, thus automating cell measurements.

An important pitfall for using the hydrodynamic focusing chip was wide channel widths (~200 microns) that occasionally caused cellular aggregation and defocussing of the cell stream from the path of laser beam. To overcome this barrier, we constructed a narrow-channel chip for simplified cell focusing in the flowing stream. We refined the microfluidic chip design for better focusing of cells through the FCS system. It is possible to achieve cell focusing using narrow channels that are capable of passing cells sequentially through the confocal volume. These chips are simpler to operate for most fluorescent probe based assays. Figure 4.6 shows the design of such a narrow channel chip, in which the channel width is similar to the size of cells (22.3 μm with a standard deviation of 1 μm). Increasing the height of these narrow channels to 40 μm minimized potential clogging of the channel due to cellular debris. The volumetric flow rate of cells pumped through a syringe pump into the narrow channel was optimized for adequate signal and cell throughput in a manner similar manner as obtained for the hydrodynamic focusing chip (table 4.1).

Figure 4.3 shows comparison of autocorrelation curves obtained at acquisition times of 20 s and 1 s respectively in static cell stained with calcein and Figure 4.4 shows the comparison under flowing conditions. It was observed that, the τ_D remained constant for static cells (Figure 4.3) whereas it changed for cells under flowing conditions (Figure 4.4). The τ_D observed for 1

s acquisition is 0.19 ms and 0.25 ms for an acquisition time of 20 s under flowing conditions. Whereas, the number of molecules obtained from the autocorrelation function, G(0) in the probe volume for 1 s and 20 s is 3 and 1 respectively. Therefore, it was observed that with increasing acquisition times, there was an increase in τ_D and decrease in N. These results were comparable to the one obtained by using the hydrodynamic focusing chip (Figure 4.4).

4.3 Validation of Fluorescence Measurements in Flowing Cells

The dye fluorescence in cells is determined by FCS to obtain the autocorrelation function and lag time (chapter 2). Additional parameters add to the FCS 3D model to incorporate correlation due to flow.

$$G(\tau) = \frac{1}{N}\left(1+\frac{\tau}{\tau_D}\right)^{-1}\left(1+\left(\frac{W_{xy}}{W_z}\right)^2\frac{\tau}{\tau_D}\right)^{-1/2} e^{-\left(\frac{\tau}{\tau_f}\right)^2\left(1+\frac{\tau}{\tau_D}\right)^{-1}}$$

where N is the average number of molecules present in the probe volume, τ_D is the diffusion time, W_{xy} and W_z are the axial and lateral dimensions of the confocal volume and τ_f is the correlation time due to flow. The background is low in the red region and can be neglected. In other cases for the blue-green region, the maximum of the autocorrelation function, G(0) can be corrected by subtracting it with the G(0) of background (without cells) to reflect the true average number of molecules. Triplet state and fluorescence fluctuation effects can be neglected in this model, as these effects are due to both movement of single cells in and out of the probe volume and single molecules inside these cells. The target 1 s acquisition time was sufficient to generate

an autocorrelation curve. In this study, we optimized the flow rate to find a balance between signal acquisition and cell throughput through the chip.

4.4 Potential Barriers and Alternative Strategies

The narrow channel chip (Figure 4.5) had certain barriers for long-term continuous measurements and the chip could not be recycled due to potential clogging problems. The 20 μm channel remained functional without clogging only for 2 hours continuously and the clogging was irreversible. There is also an increased possibility of cellular damage in these microfluidic chips due to the high backpressure conditions that arise in 20 μm channels. Tubeless microfluidic systems[14] have been developed using passive pumping methods to minimize cell rupture and shear stress while introducing the cells into the microfluidic device.

We designed an alternate chip model with multiple; parallel 20 μm channels to serve as an alternative to clogging issues (figure 4.7). This new chip was designed to reduce the backpressure during injection and to have multiple channels available as backup in case one of the channels clogs. This design allows continuous flow of cells almost indefinitely up to almost 5 h and the same chip can be recycled and reused after a 20-minute ethanol wash step. Cellular damages in the chip were low due to the small path of cells through the narrow channels.

4.5 Conclusion

This chapter gives an overview of how two microfluidic chip designs can be

used for high throughput screening of cell assays for cancer research. Furthermore, high throughput cell screening microfluidic platform can also be used as a gradient generator to carry out various cell based assays.[15,16] The hydrodynamic focusing chip can be used in cases where faster cell flow is required, while the multiple narrow channels chip can be used for cell assays that require slower flow rates. Both the chip designs will be used in combination with our FCS system for ultrasensitive detection. As we develop future cancer cell screening assays, these microfluidic designs can be modified to meet the experimental and instrumental specifications.

4.6 Reference

1. A. K. Price and C. T. Culbertson, *Anal. Chem*. 2007, 79, 2614-2621.

2. R. N. Zare and S. Kim, *Annu Rev. Biomed*. Eng. 2010, 12. 187-201.

3. G. A. Cooksey, J. T. Elliott, L. A. Plant, *Anal Chem*, 2011, 83, 3890 – 3896.

4. S. Yasuhara, Y. Zhu, T. Matsui, N. Tipirneni, Y. Yasuhara, M. Kaneki, A. Rosenzweig and J. A. Martyn, *J Histochem Cytochem.* 2003, 51, 873-885.

5. K.H. Al-Gubory, *Experimental Cell Research*. 2005, 310, 474–481.

6. K. Zand, T. Pham, A. Davila, D. C. Wallace, and P. J. Burke, *Anal. Chem.*, 2013, Just Accepted Manuscript, DOI: 10.1021/ac4010088.

7. L. Kang, B. G. Chung, R. Langer, A. Khademhosseini, *Drug Discov Today*, 2008, 13, 1-13.

8. H. Lai, P. A. Quinto, C. E. Sims, M. Bachman, G. P. Li, V. Venugopalan and N. L. Allbritton*, J. R. Soc. Interface.* 2008, 5, Suppl 2, S113-S121.

9. S. Hu, Z. Le, R. Newitt, R. Aebersold, J. R. Kraly, M. Jones, N. J. Dovichi, *Anal Chem*. 2003, 75, 3502-3505.

10. J. R. Rettig and A. Folch, *Anal Chem*. 2005, 17, 5628-5634.

11. A. R. Wheeler, W. R. Throndset, R. J. Whelan, A. M. Leach, R. N. Zare, Y. H. Liao, K. Farrell, I. D. Manger, A. Daridon, *Anal Chem.* 2003, 75, 3581-3586.

12. A. W. Tilles, H. Baskaran, P. Roy, M. L. Yarmush, M. Toner, *Biotechnol. Bioeng.* 2001, 73, 379–389.

13. M. Hamon, S. Jambovane, L. Bradley, A. Khademhosseini and J. W. Hong, *Anal. Chem*. 2013, 85, 5249–5254.

14. G. Walker and D. J. Beebe. *Lab Chip.* 2002, 2, 131–134.

15. S. Selimovic, W. Y. Sim, S. B. Kim, Y. H. Jang, W. G. Lee, M. Khabiry, H. Bae, S. Jambovane, J. W. Hong, A. Khademhosseini. *Anal. Chem*. 2011, 83, 2020–2028.

16. J. Y. Yun, S. Jambovane, S. K. Kim, S. H. Cho, E. C. Duin, J. W. Hong. *Anal Chem*. 2011, 83, 6148–6153.

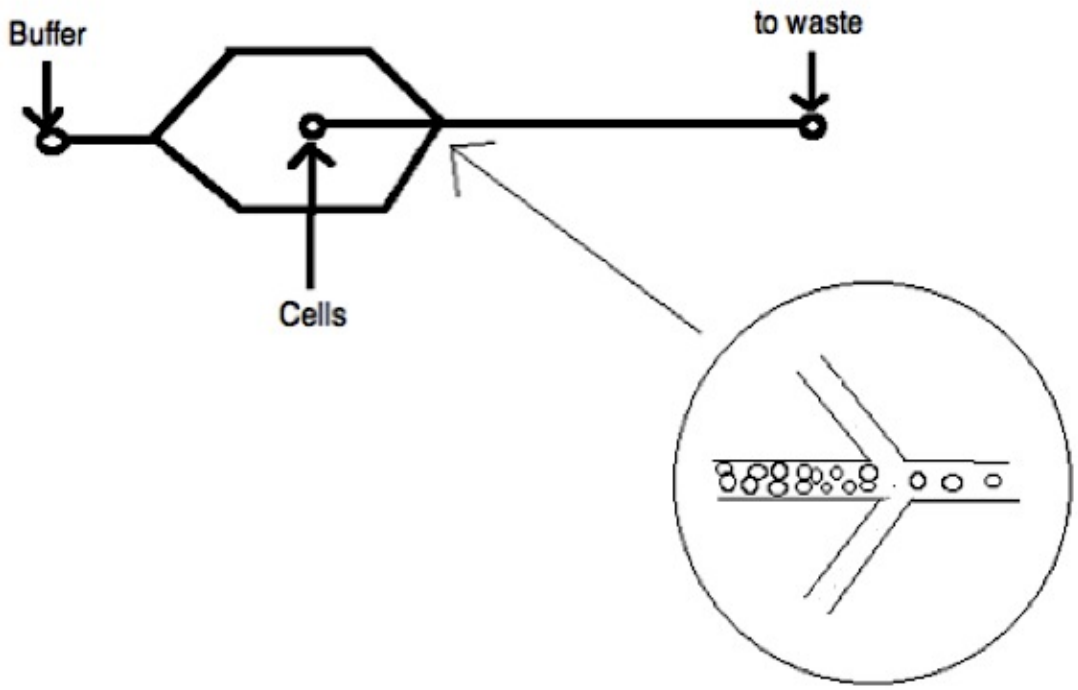

Figure 4.1: Schematic of hydrodynamic focusing single cell analysis device. Fluidic channels are dark and tubing insertion inlets are white. A focusing buffer focuses the cellular flow at the center stream. Ramos cells are pushed by the hydrodynamic flow at the junction (magnified in the figure) towards waste. This network helps formation of a single cell flow with stable trajectories from a bulk cell suspension.

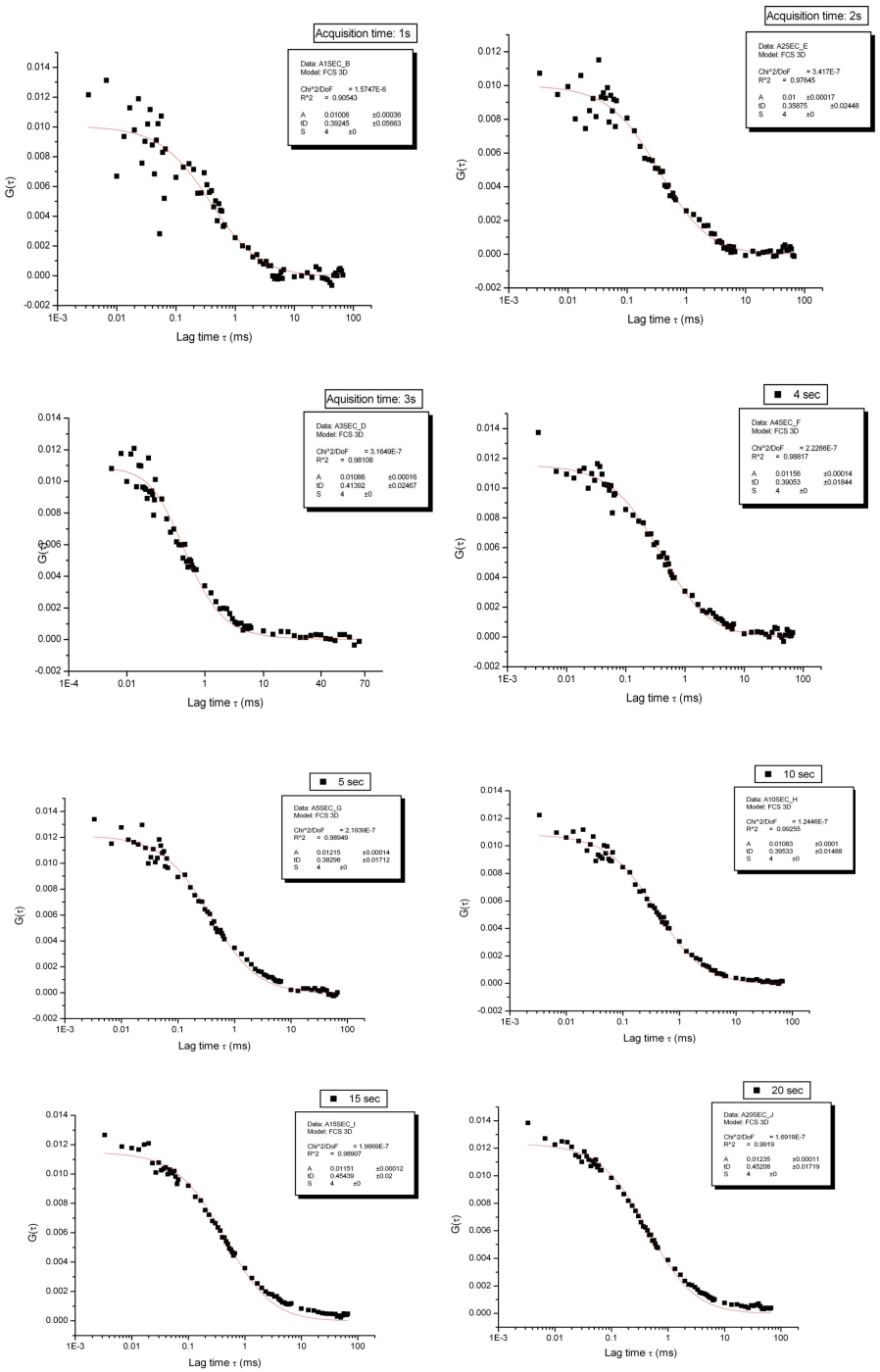

Figure 4.2: Comparison of autocorrelation curves obtained from 0.1 μM calcein stained static Ramos cells (non-flowing condition) at 1s, 2s, 3s, 4s, 5s, 10s, 15s and 20s respectively. Cell fluorescence and autocorrelation could be measured at times as small as 1 s. This preliminary test shows that the FCS acquisition time can be shortened while still measuring the autocorrelation.

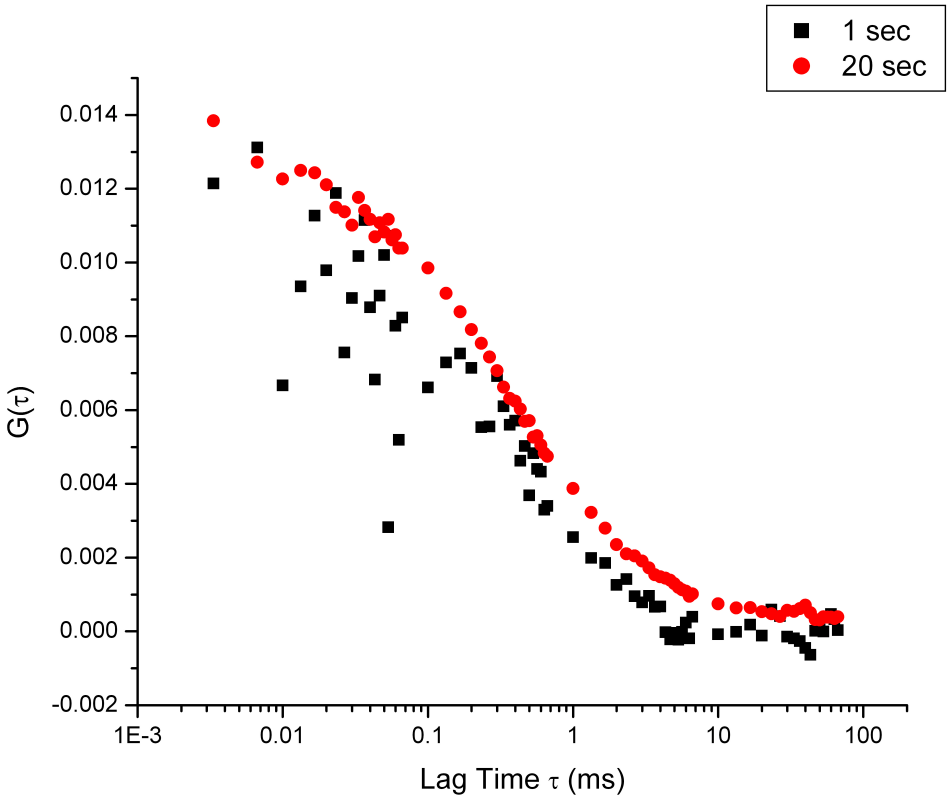

Figure 4.3: FCS signal overlay from a calcein-stained cell with 20 s and 1 s acquisition time (non-flow conditions). This is a proof of concept to show that FCS acquisition times can be shortened without compromising the diffusion times in static cells.

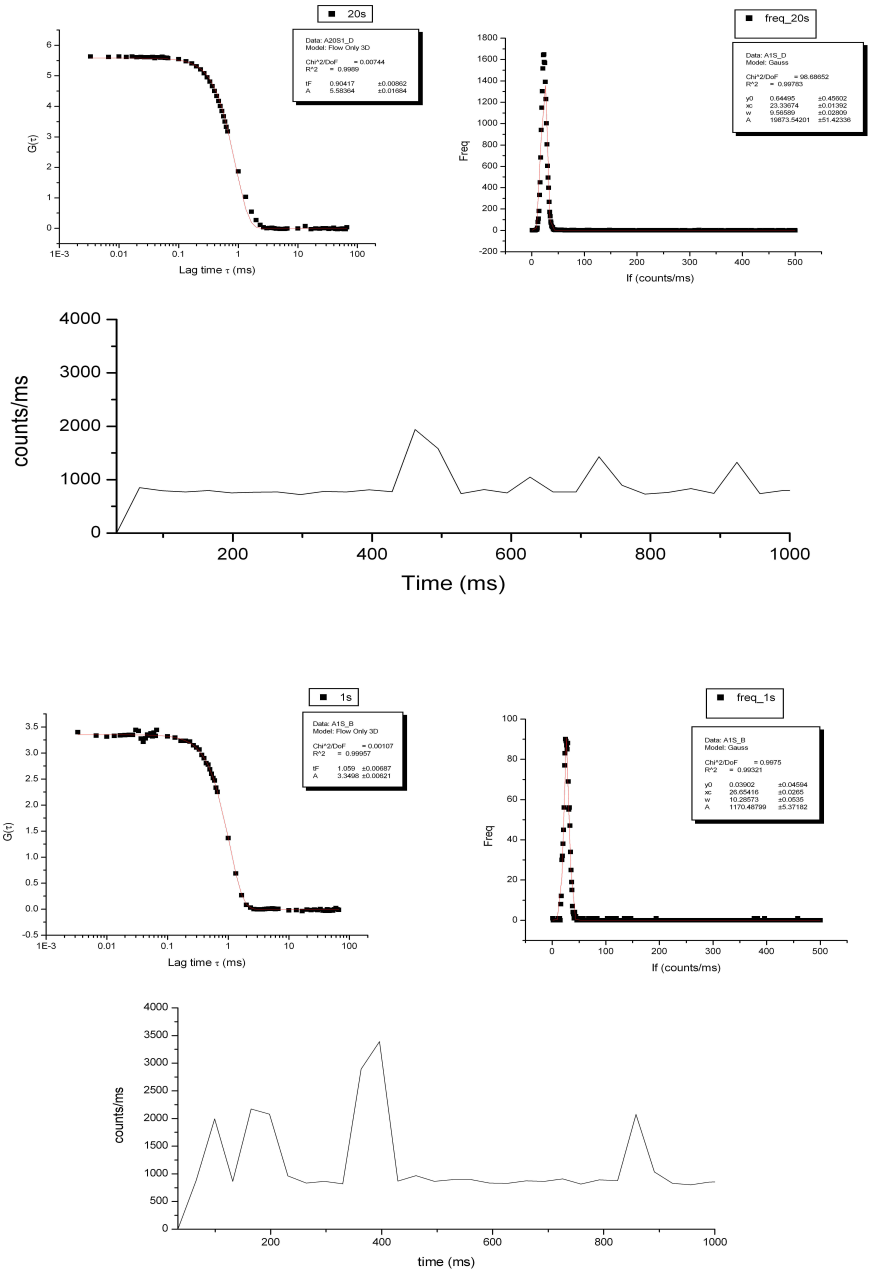

Figure 4.4: Autocorrelation curve, photon counting histogram and time trace plot of 20 s versus 1 s using FCS. Ramos cells stained with 0.1 μM calcein-AM flowing at a rate of 0.01 ml/hr and buffer rate at 0.15 ml/hr was used to measure the autocorrelated fluorescence with an FCS acquisition time as low as 1 s in the hydrodynamic focusing chip. The time trace plot shows individual calcein stained cell passing through the laser beam. Each spike represents a single cell passing through the laser beam. Residence time is around 100 ms.

The differences in intensity are due to the non-uniformity of cellular staining in the population.

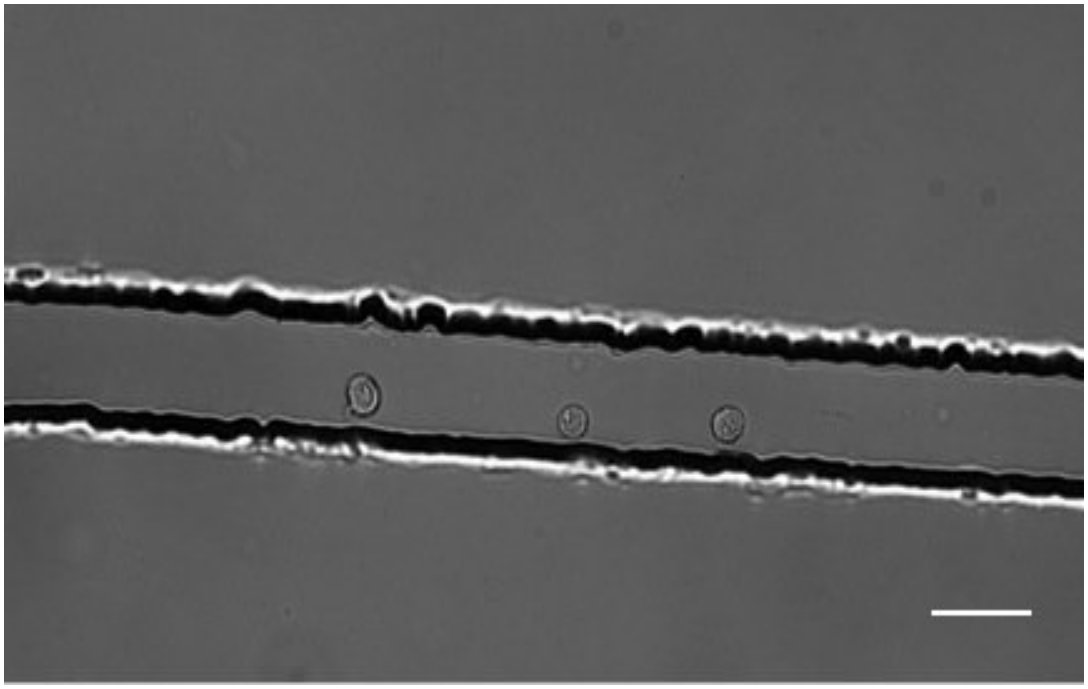

Figure 4.5: Microscope image of Ramos cells lined up in a 22.31±1 μm width (inner diameter). Cell flow rate was set to 0.01 ml/hr to set the residence time of 1 s in the beam. The channel is taller (40 μm) to reduce backpressure and clogging issues. Only cells in the detection region are measured by confocal microscopy. Whereas, cells that pass over each other will not be detected. Scale bar represents 20 μm.

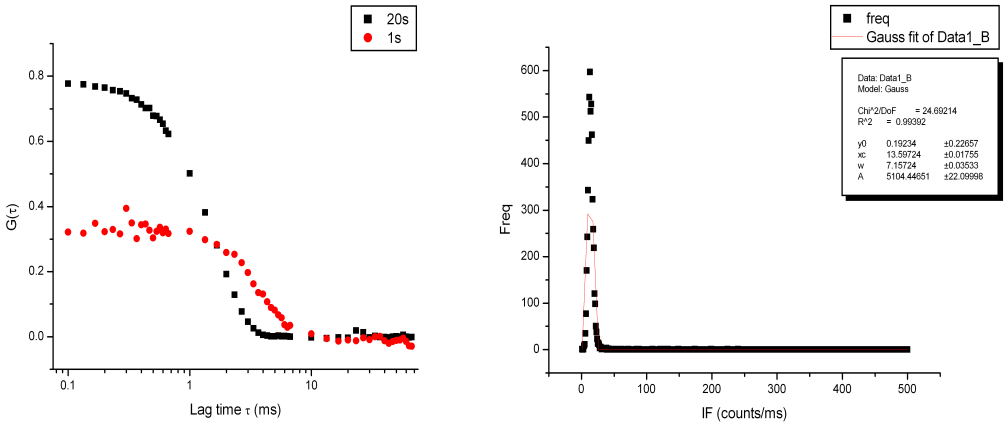

Figure 4.6: Autocorrelation of Ramos cells stained with 0.1 μM calcein-AM flowing in the narrow channel chip at a rate of 0.05 mL/hour obtained at acquisition times of 1 s and 20 s. The diffusion time was observed to be around 0.1 ms. A photon counting histogram on the right gives the average fluorescent intensity.

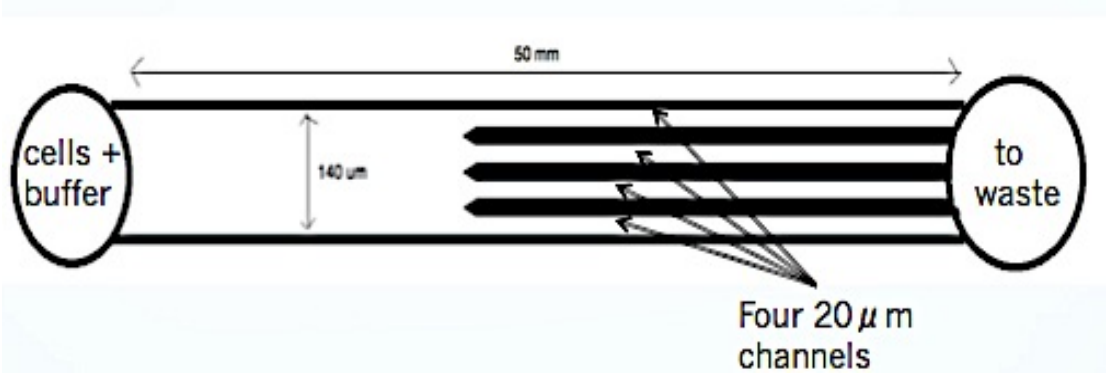

Figure 4.7: Alternative chip design with four hairline channels to reduce backpressure and include backup channels for continuous cell flow in case of clogging. This design facilitates continuous flow of cells for many hours and the chip can be recycled and reused.

Table 4.1: Summary of flow rate optimization study. The right flow rate combination of the focusing buffer and cell stream is essential for obtaining optimum signals to obtain autocorrelation curve.

Flow rate (ml/hr)	**Molecules**	**Xc**	**Flow time**
buffer / cells		counts	ms
0.15 / 0.01	2	45.47554	0.83247
0.16 / 0.01	4.5	44.00289	1.38284
0.17 / 0.01	7	43.98551	3.8457
0.18 /0.01	6	46.45312	1.21745
0.19 / 0.01	25	47.6488	1.6505
0.2 / 0.01	3	46.40885	6.45252
0.21 / 0.01	3	45.34801	11.7408
0.22 / 0.02	3	44.41944	13.00307
0.25 / 0.02	1	42.21438	13.07795
0.3 / 0.03	4	43.10583	11.24554
0.15 / 0.01	1	44.05598	15.11355

CHAPTER 5

CONCLUSION AND FUTURE DIRECTIONS

In this study, intracellular molecular mechanism such as apoptosis and pathways of inducing agents such as staurosporine and anti-CD95 has been explored. We have conducted these studies in real time by a variety of analytical techniques at early stages. However, there is a continuous need for improving the robustness and reproducibility of these analyses. Early detection of apoptosis using fluorescence microscopy and microfluidic technology has been demonstrated in this thesis to identify apoptotic cells and to study the induction kinetics of therapeutic compounds in flowing and non-flowing cells. These measurements have been performed non-invasively, with an unparalleled temporal resolution of five minutes. Moreover, the automated microfluidic based cell scanning system offers high throughput and improved cell counts for real time screening of single cells in a given analysis timeframe.

For future work, the high throughput cell assay discussed in chapter 4 can be applied to a wide array of cancer cell studies. Prior to commercial adoption of our assays, they must be implemented on a larger group of cell samples. Chapter 3 and 4 have shown studies on cancer cell response with staurosporine induction with a high temporal resolution of 5 minutes for B lymphocytes (Ramos). Similar studies can be carried out with various other cell types for a better understanding of the early induction mechanisms. The reduced autofluorescence using the MTDR probe at longer wavelengths used

in this study allows detection of apoptosis with low cell autofluorescence. New PDMS based microfluidic designs can be fabricated along with development of the optical system for method validation of these novel bioanalytical assays. Adding an optical beam splitter to the existing FCS setup, it is possible to carry out multi-color labeling of cell organelles for multi-parameter analyses and cross correlation studies using two fluorescent probes simultaneously with red and blue laser sources.

Developing an automated data processing platform will be a significant step towards high throughput analysis on the current FCS setup. A new database system in LabView can be developed to speed up the data processing to index the sample number, the stream of detected bursts and the FCS data. A limitation of flowing cell analysis on FCS is majority of analysis time spent in the absence of cells that causes scanning of the medium or buffer at low flow rates inside the microfluidic channels. Therefore, there is a necessity to reduce the unwanted data collection to reduce the overall data processing time. By collecting FCS signals from stage-scanning a cell past the laser beam burst data was obtained which was translated into FCS curves. In this case moving the cell past the laser beam via the microscope stage is less elegant than flowing the cell in a stream, but the principle is the same. Figure 5.1 shows the data obtained from stage scanning a Ramos cell past the laser beam. The cell was stained with anti-human CD71-FITC. Storing burst data that exceeds a certain threshold value in a manner similar to flow cytometry and reduces the total data burden on the computer and data

acquisition system. It may be possible to acquire data during data processing simultaneously.

As far as live cell assays are concerned, the multi-narrow channel chip discussed in chapter 4 can be readily applied to kinetic studies of several anticancer agents, providing new opportunities for automated on-chip cytometry and high throughput single cell screening. Applications of this chip design with low background noise at longer wavelength region can also be extended to a microfluidic sensor device when combined with amperometry. The sample volumes required for these analyses are as low as nano to picoliter ranges. A particular advantage of the microfluidic platform discussed in the current study lies in its ability to facilitate kinetic studies and multivariate analysis of fluorescent events in suspended cells, providing an option to interrogate cells repeatedly, which on the other hand is difficult with conventional methods. Moreover, computer simulations can be developed and utilized to model the flow behavior of cells inside these microfluidic channels.

This thesis demonstrates the combined effect of real time fluorescence analysis with state-of –the-art microfluidic technology as a highly efficient and cost effective solution for automated drug screening. This technology can also be extended to investigations into the intracellular anticancer processes. We assure that with further developments, this fluorescence microscopy combined lab-on-chip technology can successfully supplement conventional methods such as flow cytometry and fluorescence imaging plate readers.

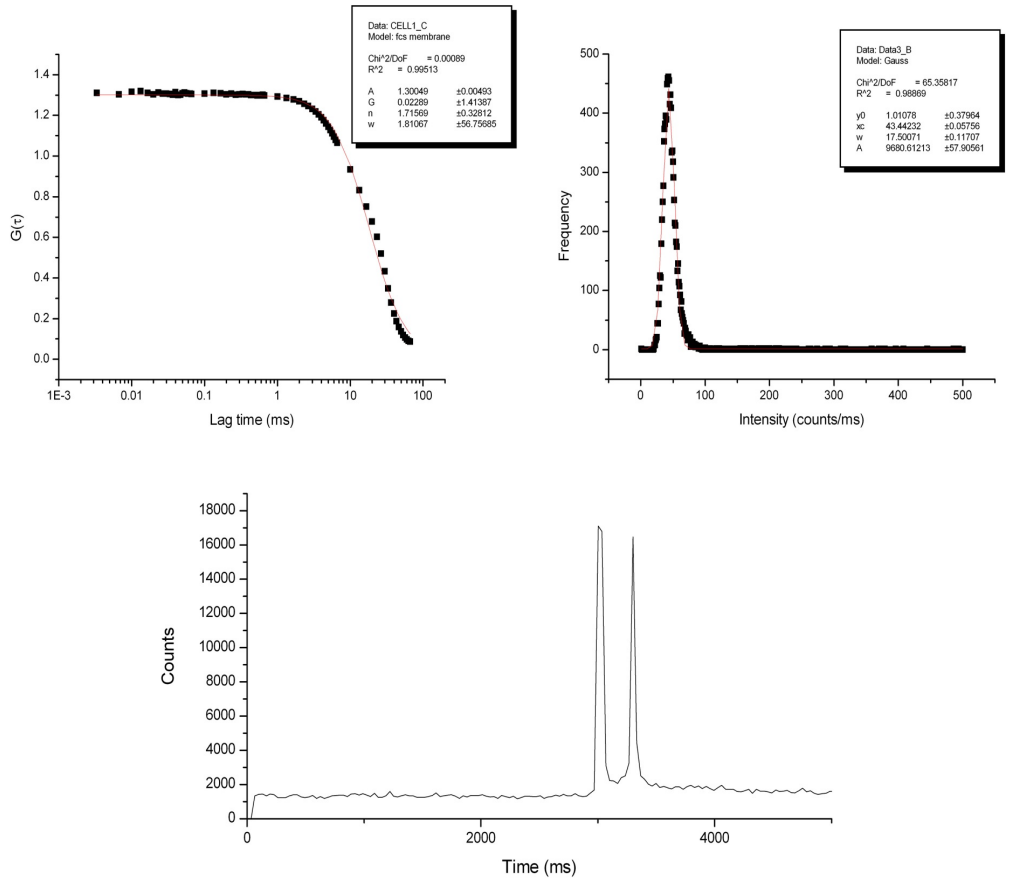

Figure 5.1: Autocorrelation curve, photon counting histogram and time trace plot obtained from single stage scanning a cell past the laser beam where the cell was stained with a fluorescein-labeled antibody for the proliferation marker CD71. The FCS curve was fit with a membrane fit model. Future software development will store bursts that only exceed a certain threshold value to reduce data burden when signals are collected over longer time periods.